# Impacts of 1.5°C and 2.0°C global warming on the onset, cessation, and length of the rainy season in global land monsoon regions

| | |
|---|---|
| Journal: | *Advances in Atmospheric Sciences* |
| Manuscript ID | AAS-2024-0386.R2 |
| Manuscript Type: | Original Article |
| Date Submitted by the Author: | 23-Jun-2025 |
| Complete List of Authors: | Taguela, Thierry; University of Illinois Chicago, Department of Earth and Environmental Sciences<br>Raji, Ibraheem; University of Illinois Chicago, Department of Earth and Environmental Sciences<br>Akinsanola, Akintomide; University of Illinois Chicago, Earth and Environmental Sciences<br>SINGHAI, PRIYANSHI ; University of Oklahoma, School of Meteorology<br>Adeyeri, Oluwafemi E.; Australian National University Fenner School of Environment and Society<br>Wainwright, Caroline M.; University of Leeds<br>Barimalala, R; Norwegian Research Center (NORCE) |
| | |

# Impacts of 1.5°C and 2.0°C global warming on the onset, cessation, and length of the rainy season in global land monsoon regions

Thierry N. Taguela[1] , Ibraheem Raji[1] , Akintomide A. Akinsanola[1,*] , Priyanshi Singhai[2] , Oluwafemi E. Adeyeri[3] , Caroline M. Wainwright[4] , Rondrotiana Barimalala[5]

1. Department of Earth and Environmental Sciences, University of Illinois Chicago, IL, USA
2. School of Meteorology, University of Oklahoma, Norman, OK, USA
3. ARC Centre of Excellence for the Weather of the 21st Century, Fenner School of Environment and Society, The Australian National University, Canberra, Australian Capital Territory, 2600, Australia.
4. University of Leeds, Leeds, UK
5. NORCE, Bergen, Norway



**Abstract**

The onset, cessation, and length of the rainy season are crucial for global water resources, agricultural practices, and food security. However, the response of precipitation seasonality to global warming remains uncertain. In this study, we analyze how global warming levels (GWLs) of 1.5°C and 2°C could affect the timing of rainfall onset (RODs), rainfall cessation (RCDs), and the overall duration of the rainy season (LRS) over global land monsoon (GLM) regions using simulations from the Coupled Model Intercomparison Project Phase 6 (CMIP6) under the SSP2–4.5 and SSP5–8.5 scenarios. With high model consensus, our results reveal that RODs are projected to occur later over South Africa (SAF), North Africa (NAF), and South America (SAM) but earlier over South Asia (SAS) and Australia (AUS) in a warmer climate. The projected early RODs in AUS are more pronounced at 2°C GWL under the SSP5–8.5 scenario. On the other hand, early RCDs are projected over SAM and East Asia, while late RCDs are projected over NAF with high inter-model agreement. These changes are associated with a future decrease in LRS in most GLM regions. Additionally, we found that continuous warming over 1.5°C will further reduce the length of the rainy season, especially over the SAM, NAF, and SAF monsoon regions. The findings underscore the urgent need to mitigate global warming.

**Keywords:** Rainfall onset, Rainfall cessation, Global land monsoon, Rainy season length, CMIP6 Projections, Global warming levels

*Corresponding author: Akintomide A. Akinsanola (aakinsan@uic.edu)

https://doi.org/10.1007/s00376-025-4386-9

**Article Highlights:**

- Future RODs over South Africa, North Africa, and South America are likely to be delayed, while early RCDs are projected over South America.
- Changes in RODs and RCDs are associated with a future decrease in LRS in most GLM regions.
- Continuous warming over 1.5°C will further reduce LRS, particularly in the monsoon regions of South America, North Africa, and South Africa.

## 1. Introduction

The global land monsoon (GLM) system comprises seven major monsoon regions: North America (NAM), South America (SAM), North Africa (NAF), South Africa (SAF), South Asia (SAS), East Asia (EAS), and Australia (AUS) (Yim et al., 2014; P. Wang et al., 2017; Wang et al., 2020). These regions are characterized by a seasonal reversal of wind direction driven by differential heating between land and ocean surfaces, leading to enhanced moisture transport and a pronounced increase in precipitation during the local summer season (Akinsanola & Zhou, 2018, 2020; Chen et al., 2020; Chakraborty and Singhai, 2021). The monsoon system plays a critical role in global hydrological and energy cycles, directly influencing the livelihoods, water resources, and agricultural productivity of nearly two-thirds of the world's population (Wang et al., 2012; Kitoh et al., 2013; Akinsanola & Zhou, 2018; W. Zhang et al., 2018; Wang and Ding, 2008; Zhang & Zhou, 2019a). However, these regions exhibit high sensitivity to global climate change, as warming-induced shifts in atmospheric circulation and moisture availability can alter monsoon intensity, duration, and variability (Seager et al., 2010; Kitoh et al., 2013; Zhang & Zhou, 2019b; Zhou et al., 2020). Given the profound socioeconomic and ecological consequences of monsoon variability, robust and reliable projections of GLM precipitation characteristics are essential for improving climate adaptation and mitigation strategies in these vulnerable regions.

Over the past 30 years, the average global surface temperature has risen by about 0.2°C per decade due to increased greenhouse gas concentrations, driven mainly by anthropogenic factors (IPCC, 2021). Studies have shown that this warming trend has a major impact on the hydrological cycle (Donat et al., 2016; Lehmann et al., 2015; Mishra and Liu, 2014), altering precipitation characteristics in GLM regions (Vera et al. 2006; Jones & Carvalho, 2013; Kitoh et al. 2013; Ni and Hsu 2018; Akinsanola & Zhou, 2018; Zhang et al. 2018; Deng et al. 2018; Zhang and Zhou 2019b; Seth et al. 2019; Moon and Ha 2020; Akinsanola & Zhou, 2020; Wang et al. 2020; Chen et al. 2020; Chang et al., 2022). For example, more frequent severe rainfall extremes have been documented in the Australian and South American monsoon regions (Wang et al., 2020; Jones & Carvalho, 2013). Over South Asia, precipitation shows decreased occurrence of low and moderate intensities triggering meteorological drought (Mishra and Liu, 2014), with an increasing positive trend in summer monsoon precipitation over the northern parts of India's west coast (Preethi et al., 2017). The summer monsoon rainfall in South Asia has been consistently projected to rise (Menon et al., 2013; Sharmila et al., 2015; Kitoh et al., 2013), while in North America, it will likely decrease (Jin et al., 2020). Regionally, because of the disparity in warming rates between hemispheres, projected changes in monsoon precipitation show a more significant and consistent increase in the Northern Hemisphere (NH) compared to the Southern Hemisphere (SH) (Lee & Wang, 2014). Earlier research has found that, under severe climate scenario pathways, there is a projected rise in the frequency of floods and droughts in eastern Africa (Ayugi et al. 2021). Future projections indicate a decrease in precipitation across both North and South Africa, with North Africa experiencing notably wet years and South Africa facing significantly drier years by the end of the 21st century (Majdi et al., 2022; Almazroui et al., 2020; Bobde et al., 2024). Given these significant alterations in precipitation patterns, it is important to draw more attention to the timing of rainfall onset and cessation, along with the length of the rainy season to enhance our understanding and preparedness for the resulting hydrological impacts.

Although future GLM changes have received much attention, most studies have focused on understanding and predicting precipitation characteristics such as mean and extreme rainfall (e.g., Akinsanola & Zhou, 2019; Jin et al., 2020; Chen et al., 2020; Yao et al., 2021; Liu et al., 2022; Das et al., 2022; Chang et al., 2022), with limited attention to changes in onset and cessation dates of the rainy season. However, understanding the impact of global warming on these rainy season characteristics in GLM regions is vital for developing adaptive strategies in socioeconomic sectors such as agriculture, water resource management, and disaster preparedness (Turner & Annamalai, 2012). Early or delayed onset can significantly affect crop planting schedules and yields, while premature or prolonged cessation impacts water availability and increases the risk of droughts and floods (Gadgil & Gadgil, 2006; Dash et al., 2007; Sylla et al., 2016; Singhai et al, 2023). Findings from studies reveal that higher warming levels could trigger a delayed rainfall onset and early withdrawal due to variations in atmospheric circulation patterns and gradients of sea surface temperatures (Kitoh et al., 2013; Khadka et al., 2021). For instance, a projected average delay of 5–10 days in the start of the wet season in West Africa, along with a later onset in South Africa, is linked to the intensifying Saharan heat low during late summer and a northward shift in the tropical rain belt from August to December (Dunning et al., 2018). Furthermore, Khadka et al. (2021) observed that most CMIP5 and CMIP6 models predict a late onset and early retreat for the Southeast Asian monsoon. However, under a high-emission scenario, CMIP6 models project an earlier summer monsoon onset over the Arabian Sea and a delayed onset over the Bay of Bengal and South China Sea, driven by shifts in the northward migration of the equatorial intraseasonal oscillation (Wang et al., 2024). Moreover, Cheng et al. (2024) identified a significant correlation between delayed monsoon onset projections over the Bay of Bengal/South China Sea and western Pacific sea surface temperature (SST) simulations, prompting adjustments that halved the projected delay. On the other hand, the projected duration of the Indian summer monsoon (ISM) shows reduced uncertainty when constrained by observed SST trends in the western Pacific and surface warming trends over the northern mid-high latitudes, suggesting a 6-day reduction in ISM duration under a high-emission scenario (Cheng et al., 2025). Additionally, based on observations and CMIP5 models, Hariadi et al. (2021) showed that the El Niño–Southern Oscillation (ENSO) influences the monsoon's onset and cessation dates in Southeast Asia, with El Niño events causing an early onset, and La Niña events leading to a delayed onset. Similarly, more erratic onset and cessation patterns (Omondi et al., 2014), along with the duration of the rainy season (Sabeerali & Ajayamohan, 2018), are expected to be more pronounced toward the end of the 21st century.

Despite these significant advances in monsoon research, most studies have focused predominantly on individual regional monsoon systems, leaving a critical gap in our understanding of how rainy season characteristics respond to global warming at the broader GLM scale. Specifically, the response of key monsoon attributes—such as rainfall onset dates (RODs), cessation dates (RCDs), and the length of the rainy season (LRS)—to future climate scenarios remains insufficiently explored across all GLM regions. Furthermore, limited research has systematically assessed how these characteristics evolve under different levels of global warming, particularly the 1.5°C and 2.0°C thresholds outlined in the Paris Agreement. Given the substantial societal and ecological dependence on monsoon rainfall, it is crucial to comprehensively evaluate the spatially heterogeneous impacts of climate change on monsoon dynamics. This study builds on previous studies to provide a comprehensive assessment of projected changes in RODs, RCDs, and LRS under varying warming scenarios across all GLM regions, offering critical insights for climate adaptation strategies and water resource management.

CMIP6 models are used to assess changes based on the Shared Socioeconomic Pathway (SSP) 2–4.5 and 5–8.5 scenarios. The rest of this paper is organized as follows: Section 2 details the data and methods employed in the study. Section 3 assesses how well the model simulates the climatology of onset dates, cessation dates, and length of the rainy season over GLM regions. Section 4 investigates projected changes in the onset, cessation, and duration of the rainy season, along with changes in key rainfall characteristics, including total rainfall, rainfall per rainy day, and the number of rainy days. Finally, section 5 presents a summary and conclusions.

## 2. Data and Methods

This study uses historical and future precipitation datasets from 16 CMIP6 (Coupled Model Intercomparison Project Phase 6) models (Eyring et al., 2016), as detailed in Table S1. These datasets encompass the historical period (1995–2014) as defined in the Intergovernmental Panel on Climate Change (IPCC) Sixth Assessment Report (AR6), and the future (2015–2100). The study employs the SSP2–4.5 and SSP5–8.5 scenarios, reflecting moderate mitigation and worst-case scenarios. Moderate mitigation efforts are anticipated in the SSP2–4.5 scenario, potentially limiting global warming to approximately 2.5°C above pre-industrial levels by the end of the 21st century (O'Neill et al., 2017). Conversely, the SSP5–8.5 scenario, also known as "business as usual," depicts a future with high fossil fuel use and limited efforts in climate mitigation, resulting in an approximate 5°C increase in temperature by the close of the 21st century. The first realization (r1i1p1f1) is used in each model's historical and future projections to maintain consistency in the analysis. The study also explores the warming thresholds of 1.5°C and 2.0°C compared to pre-industrial levels. These thresholds are identified as the initial year when the 21-year running mean of the global mean surface temperature (GMST) arrives at 1.5°C and 2.0°C above pre-industrial levels. Two 10-year periods around each threshold are selected (Hauser et al., 2021; Ayugi et al., 2022). Table 1 presents the timing of reaching 1.5°C and 2.0°C of global warming relative to pre-industrial levels under the SSP2–4.5 and SSP5–8.5 scenarios. The CMIP6 multi-model ensemble mean approach (referred to here as "EnsMean") is employed to address systematic biases due to model differences (Akinsanola & Zhou, 2018). The historical performance of the CMIP6 models, along with their EnsMean, is evaluated using observed daily datasets from the unified gauge-based analysis of global daily precipitation (CPC) at 0.5°×0.5° resolution (Xie et al., 2010). In addition, we use CPC data to identify the land areas of the global monsoon (GM) domain. Following Wang et al. (2012) and Chen et al. (2020), we defined the GM domain as the area where the precipitation difference between local summer and winter exceeds 2.0 mm/day, and local summer precipitation accounts for more than 55% of the annual total precipitation. Summer here refers to May to September for the Northern Hemisphere (NH) and November to March for the Southern Hemisphere (SH).

To compare all datasets, we remap them using first-order conservative remapping onto a common spatial grid of 2.81° × 2.81°, adhering to the lowest model resolution following Faye & Akinsanola

(2021) and Akinsanola et al. (2024, 2025). Next, the metrics (e.g., onset date) are calculated for each model and averaged to obtain the EnsMean of the models. Assessing model performance in simulating historical precipitation is crucial for identifying uncertainty sources and enhancing confidence in future projections. Here, CMIP6 models are evaluated against observations using the percentage bias (Eq.1), normalized root mean square error (NRMSE: Eq.2), pattern correlation coefficient (PCC: Eq.3), and Taylor skill score (TSS: Eq.4). Results are summarized through portrait diagrams, providing a clear comparison of model performance across all monsoon regions (Akinsanola et al., 2021; Taguela et al., 2025).

$$\%BIAS = \frac{\sum_{i=1}^{n}(M_i - O_i)}{\sum_{i=1}^{n} O_i} \times 100 \quad (1)$$

$$NRMSE = \frac{\sqrt{\frac{1}{n}\sum_{i=1}^{n}(M_i - O_i)^2}}{\frac{1}{n}\sum_{i=1}^{n} O_i} \quad (2)$$

$$PCC(M, O) = \frac{cov(M,O)}{\sqrt{Var(M) \times Var(O)}} \quad (3)$$

$$TSS = \frac{4(1+PCC)^2}{\left(\frac{\sigma M}{\sigma O} + \frac{\sigma O}{\sigma M}\right)^2 (1+PCC_0)^2} \quad (4)$$

where "O" and "M" are observation and reference model means, respectively; "cov" stands for covariance while "var" is variance; and "$n$" is the total number of time steps. The standard deviation is denoted by σ, while $PCC_0$ represents the highest possible value of PCC, set to 1. The TSS varies between 0 and 1, indicating no match or a perfect match between the model and the observations. Numerous studies have employed TSS to evaluate model performance (e.g., Faye and Akinsanola, 2021; Bobde et al., 2024).

**Table 1:** Timing of each CMIP6 model for reaching 1.5°C and 2.0°C GWLs under the SSP2–4.5 and SSP5–8.5 scenarios (Hauser et al., 2021).

| | **SSP2–4.5** | | **SSP5–8.5** | |
|---|---|---|---|---|
| **Model Name** | **GWL 1.5°C** | **GWL 2.0°C** | **GWL 1.5°C** | **GWL 2.0°C** |
| ACCESS-CM2 | 2019-2038 | 2031-2050 | 2016/2035 | 2029-2048 |

| | | | | |
|---|---|---|---|---|
| ACCESS-ESM1-5 | 2020-2039 | 2036-2055 | 2018-2037 | 2030-2049 |
| CanESM5 | 2004-2023 | 2015-2034 | 2003-2022 | 2013-2032 |
| CESM2-WACCM | 2015-2034 | 2030-2049 | 2011-2030 | 2024-2043 |
| CMCC-CM2-SR5 | 2016-2035 | 2029-2048 | 2012-2031 | 2024-2043 |
| CMCC-ESM2 | 2021-2040 | 2031-2050 | 2020-2039 | 2030-2049 |
| EC-Earth3 | 2013-2032 | 2035-2054 | 2015-2034 | 2026-2045 |
| INM-CM4-8 | 2026-2045 | 2054-2073 | 2021-2040 | 2037-2056 |
| INM-CM5-0 | 2028-2047 | 2063-2082 | 2021-2040 | 2037-2056 |
| IPSL-CM6A-LR | 2009-2028 | 2024-2043 | 2009-2028 | 2025-2044 |
| MIROC6 | 2037-2056 | 2064-2083 | 2031-2050 | 2044-2063 |
| MPI-ESM1-2-HR | 2028-2047 | 2054-2073 | 2024-2043 | 2040-2059 |
| MPI-ESM1-2-LR | 2027-2046 | 2048-2067 | 2025-2044 | 2039-2058 |
| MRI-ESM2-0 | 2021-2040 | 2040-2059 | 2017-2036 | 2029-2048 |
| NESM3 | 2015-2034 | 2033-2052 | 2011-2030 | 2024-2043 |
| TaiESM1 | 2022-2041 | 2034-2053 | 2019-2038 | 2027-2046 |



The onset and cessation dates are determined using the approach outlined by Liebmann and Marengo (2001), with adjustments introduced by Bombardi et al. (2019). The method uses only precipitation data and has been applied across the global monsoon region by Wainwright et al. (2021) and Bombardi and Boos (2021). The daily accumulation of precipitation anomalies (*S*), beginning from the dry season, is used to detect onset and cessation dates. Based on the region's climatology, *S* defines a threshold that accounts for the persistence of precipitation leading up to these dates. The onset date is identified when *S* reaches a local minimum, while the cessation date is determined retrospectively by applying the same calculation from the year's end backward. *S* is calculated using Equation 5.

$$S = \sum_{i=t_0}(P_i - \overline{P}) \qquad (5)$$

where $P_i$ represents the amount of precipitation measured daily on day $i$; $\overline{P}$ denotes the mean annual precipitation rate over a long term, measured in mm/day; and $t_0$ marks the beginning date for the computations. It should be noted that this method does not consider areas with two or three wet seasons annually. This is achieved by analyzing the proportion of variance explained by the initial three harmonics of the mean annual precipitation cycle. If the second or third harmonic accounts for as much variance as the first harmonic or more, it suggests a pronounced bimodal or trimodal precipitation regime, leading to the region being masked (Bombardi et al., 2019). The duration of the rainy season is defined as the period between the start and end dates of rainfall. We also assess potential future changes in the frequency and intensity of rainfall during the season, defining a rainy day as having more than 1 mm of precipitation, in line with the criteria used in CLIMDEX indices (Zhang et al., 2011). The average precipitation during these wet days is then computed to represent the intensity of heavy rainfall (Dunning et al. 2018).

The projected changes are determined by comparing the 20-year time slice from the projection (see Table 1 for the period) with the historical period (1995–2014), and future changes are deemed robust when a minimum of 70% of individual models align on the direction or sign of the ensemble mean. To evaluate the possibility of mitigating the effects of reaching 2.0°C above pre-industrial levels, the avoided impacts caused by an extra 0.5°C increase in warming are calculated using equation (6):

$$\text{Avoided Impacts} = \left(\frac{GW_{2.0} - GW_{1.5}}{GW_{2.0}}\right) \times 100\% \quad (6)$$

$GW_{1.5}$ and $GW_{2.0}$ represent the changes associated with 1.5°C and 2.0°C warming compared to the historical period. This method has been employed in several recent studies (e.g., Wang et al., 2020; Chen et al., 2020; Ayugi et al., 2022).

## 3. Mean climatology of onset, cessation, and length of the rainy season

We begin by evaluating the capability of CMIP6 models to reproduce the climatological mean of RODs, RCDs, and LRS across GLM regions by comparing model outputs with CPC observations (Figure 1). Observations indicate that RODs typically occur during boreal (austral) spring, whereas RCDs generally take place during boreal (austral) fall (Figure 1a,d) in the Northern (Southern) Hemisphere. This seasonal pattern is driven primarily by the latitudinal migration of the Intertropical Convergence Zone (ITCZ), which modulates convection throughout the year (Nicholson, 2018; Daron et al., 2019). However, mesoscale circulations, orographic influences, and land-use changes also contribute to regional variations in the timing of rainfall onset and cessation (Mugalavai et al., 2008; Atiah et al., 2021; Amekudzi et al., 2015; Omay et al., 2023; Mwangi et al., 2024). While some monsoonal regions exhibit significant spatial variability in RODs and RCDs, others display more consistent seasonal characteristics. For example, in the NAF monsoon region, RODs exhibit a zonally consistent northward progression, beginning along the coast in late March (Julian Day ~90) and reaching ~18°N by mid-June (Julian Day ~170) (Figure 1a). This pattern aligns with that found by Kumi and Abiodun (2018), who analyzed the historical RODs, RCDs, and LRS over West Africa using CHIRPS (Hazard Group Infrared Precipitation with Stations) and ARC2 (African Rainfall Climatology version 2) observations. Although moisture transport in this region also originates from the Mediterranean and the Indian Ocean (Adeyeri et al., 2024), the northward progression of RODs is driven primarily by the northward transport of moisture by the West African Monsoon, which advects moisture from the Gulf of Guinea into the subcontinent (Omotosho et al., 2000; Sylla et al., 2013; Akinsanola and Zhou, 2020). In contrast, the spatial distribution of RODs and RCDs is more homogeneous across NAM and EAS (Figure 1a,d), except in the southeastern part of EAS, where RODs occur significantly earlier than in other parts of the region (Figure 1a).

EnsMean generally captures the key spatial climatology of RODs (Figure 1b) and RCDs (Figure 1e) across GLM regions. However, compared to observations, EnsMean exhibits a systematic delay in RODs of approximately 20–30 days over SAS and 10–20 days over eastern SAM and northern NAM, while advancing RODs by 20–30 days over NAF and EAS (Figure 1c). In contrast, the simulated RCDs show lower biases than the RODs (Figure 1f), with an advance of about 10–15 days over NAF and NAM and a delay of approximately 10 days over AUS.

Regarding LRS, observations indicate that among the monsoon regions, SAM experiences the longest LRS (>160 days), while SAS has the shortest (<90 days) (Figure 1g). This spatial pattern is relatively well captured by EnsMean (Figure 1h), though biases in duration remain (Figure 1i). Specifically, EnsMean overestimates LRS by up to 30 days over eastern NAF, primarily due to earlier RODs (Figure 1c). Additionally, a positive bias of about 15 days is observed over EAS, while SAS exhibits a negative bias of approximately 10 days. A distinct dipole bias emerges in the SAM region, with LRS overestimated by roughly 20 days in the western part and underestimated by a similar margin in the eastern part.

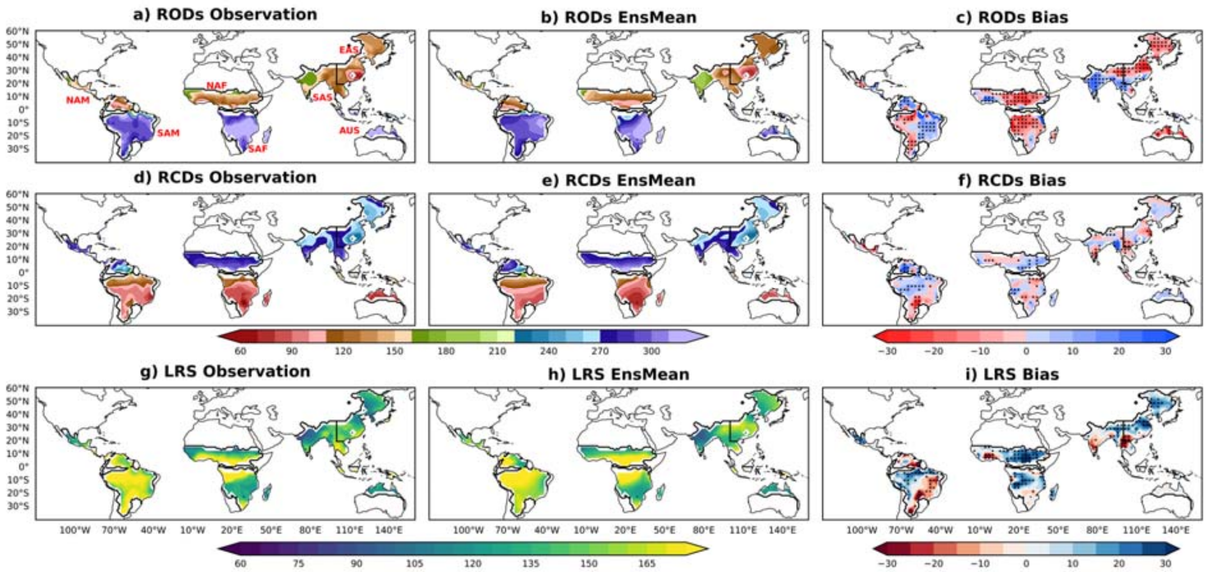


*Figure 1: The climatological mean (1995–2014) for (a-c) rainfall onset dates (RODs), (d-f) rainfall cessation dates (RCDs), and (g-i) length of the rainy season (LRS), measured in Julian days. The figures represent (a, d, g) observational data, (b, e, h) the CMIP6 EnsMean, and (c, f, i) biases of EnsMean relative to observations (measured in days). Areas with stippling in (c, f, i) are regions where differences are statistically significant at the 95% confidence level according to the Student's t-test. The black contour line outlines the GLM domains, including North America (NAM), North Africa (NAF), South America (SAM), South Africa (SAF), East Asia (EAS), South Asia (SAS), and Australia (AUS).*

Additionally, we evaluate the performance of individual models in reproducing the mean climatology of RODs, RCDs, and LRS across each monsoon region, and the results are presented using portrait diagrams illustrating the percentage bias, NRMSE, PCC, and TSS. These metrics measure the differences between the climatological mean of the observations and models (Figure 2). Previous studies have demonstrated the effectiveness of these diagrams (e.g., Akinsanola et al., 2021; Taguela et al., 2020; Bobde et al., 2024). A desirable outcome is to have a low percentage bias and NRMSE, along with high values for PCC and TSS (Bobde et al., 2024; Akinsanola et al., 2024). Figure 2 shows that, across the GLM regions, CMIP6 models have difficulty simulating RODs (Figure 2a) compared to RCDs (Figure 2b). This is indicated by the higher percentage bias values for RODs relative to RCDs, with values as large as -26% in the NAF region for models such as INM-CM5-0 (Figure 2a), leading to a high LRS percentage bias of 25% (Figure 2c). The models' NRMSE values (Figure 2d-f) are relatively low across most monsoon regions, except over AUS, where the NRMSE values for RODs, RCDs, and LRS are higher, with most models showing values between 0.5 and 0.7. Positive PCC values are generally observed (Figure 2g-i), with most models reaching up to 0.8–0.9 in SAS for RODs and RCDs, and in NAF and AUS for LRS. The

TSS for RODs, RCDs, and LRS indicates regional variations across models (Figure 2j-l). AUS exhibits the lowest scores for RODs (Figure 2j) and the highest for LRS (Figure 2l), while SAS shows the highest scores for RCDs, reaching 0.9 for most models (Figure 2k). Overall, while some individual models display significant biases, EnsMean consistently outperforms most individual models across all variables (RODs, RCDs, and LRS) and evaluation metrics (percentage bias, NRMSE, PCC, and TSS). This highlights EnsMean as a more reliable choice for further analysis and discussion over GLM regions.

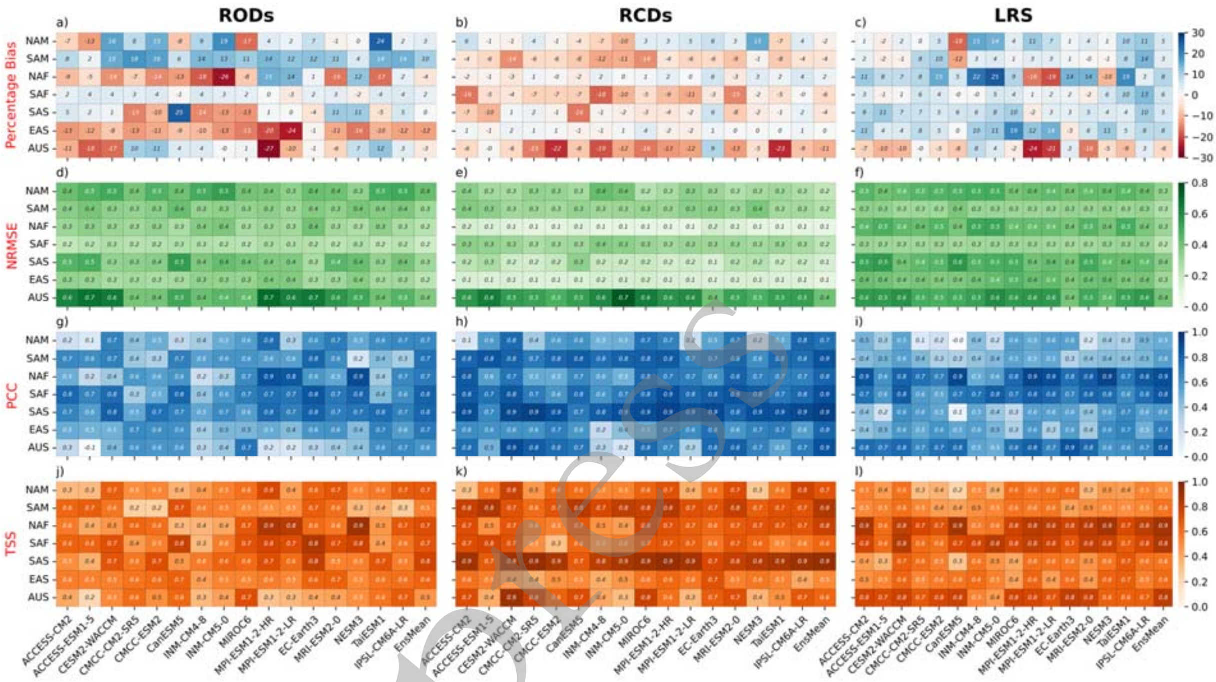


*__Figure 2:__ Portrait diagrams showing the (a-c) percentage bias (unit: day), (d-f) normalized root mean square error (NRMSE), (g-i) pattern correlation coefficient (PCC; %), and (j-l) Taylor skill score (TSS) of the (a, d, g, j) rainfall onset dates (RODs), (b, e, h, k) rainfall cessation dates (RCD), and (c, f, i, l) rainy season length (LRS) in each GLM region for individual models, along with the CMIP6 EnsMean compared with CPC during the 1995-2014 period.*



## 4. Changes in rainy season characteristics

### 4.1 Projected changes in the onset, cessation, and length of the rainy season

The projected changes in RODs, RCDs, and LRS over GLM regions under the SSP2–4.5 and SSP5–8.5 scenarios are shown in Figure 3 for different global warming levels. Earlier RODs are projected over EAS (about 4 days earlier at 2.0°C under the SSP2–4.5 scenario). Projected RODs in EAS align with results from Ha et al. (2020). However, across most GLM regions, regardless of scenario or warming level (Figure 3a, d, g, j), EnsMean generally projects a delay in future RODs. This agrees with findings from Dwyer et al. (2014), Dunning et al. (2018), and Wainwright et al. (2021). The delays in future RODs could be attributed to reduced latent heat fluxes linked to negative soil moisture anomalies (Collini et al. 2008). These delays increase with continuous warming, reaching 4-5 days under SSP2–4.5 and 6-7 days under SSP5–8.5 in NAF, SAF, and SAM at the 2.0°C global warming level (Figure 3j). The projected delay in RODs is particularly robust over SAM and SAF, with at least 70% of the models agreeing on the sign of the change in EnsMean across these regions. Additionally, models show relatively low uncertainty in the projected changes in RODs across SAM, with spreads ranging from -1 to 5 days under the 2°C warming level for both scenarios (Figure 4b, 5b, and S3b). The highest uncertainties in the projected RODs (±15 days) are observed over AUS (Figure S3g), where EnsMean projects advanced RODs under both scenarios (Figure 3a, d, g, j). This advancement is more pronounced under 2.0°C global warming, reaching up to 10 days under the SSP5–8.5 scenario (Figure 3j). For projected changes in RCDs (Figure 3b, e, h, k), delays (advancements) are observed under all scenarios and warming levels over NAF (SAM), reaching 5 to 6 (4 to 5) days under SSP5–8.5 at the 2.0°C warming level (Figure 3k). These delays in RCDs are robust over NAF, with strong model consensus. All scenarios also project an advancement of approximately 5 days (2 days) over NAM (AUS). However, the highest uncertainties in projected RCDs are found over NAM, with model spreads between -10 and 10 days (Figures 4a, 5a, S1a-S3a), while the lowest uncertainties are over EAS, with spreads between -3 and 3 days (Figures 4f, 5f, S1f-S3f).

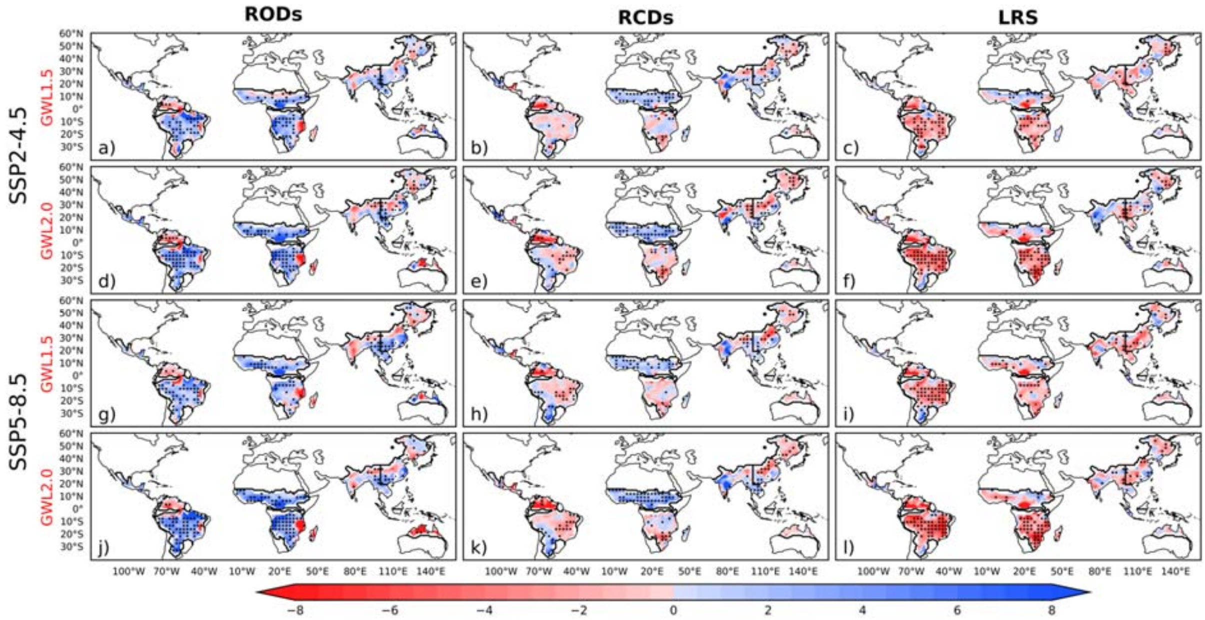


***Figure 3:*** *Future changes in rainfall onset dates (RODs), rainfall cessation dates (RCDs), and length of the rainy season (LRS) across GLM regions, compared to the 1995-2014 period based on the CMIP6 EnsMean under the SSP2–4.5 and SSP5–8.5 scenarios at various global warming levels. (a–c) SSP2–4.5/1.5ºC, (d–f) SSP2–4.5/2.0°C, (g–i) SSP5–8.5/1.5°C, and (j–l) SSP5–8.5/2.0°C. Stippling marks areas where at least 70% of the models concur on the direction of change in EnsMean.*

Under the combined impacts of changes in RODs and RCDs, LRS is expected to decrease over SAM and SAF under both the SSP2–4.5 and SSP5–8.5 scenarios (Figure 3c, f, i, and l), with a pronounced decrease (>8 days) under 2.0°C global warming in each scenario. This is likely related to the projected delays in RODs in these regions (Figure 3a, d, g, j). Although the shortening in LRS over SAF shows strong model consensus only under 2.0°C warming in each scenario (Figure 3f and 3l), the decrease over SAM is robust under both 1.5°C and 2.0°C warming in both scenarios. Although some studies suggest a rise in LRS of the East Asian monsoon (Kitoh et al., 2013; Lee & Wang, 2014; Moon & Ha, 2020), consistent with Sabeerali & Ajayamohan (2018) and except at 2°C under SSP2–4.5, a projected decrease in LRS is also observed over SAS and EAS. Sabeerali & Ajayamohan (2018) attributed this decrease primarily to the warming of the western Indian Ocean, which reduces the upper-tropospheric temperature gradient and consequently reduces LRS. Uncertainties in the projected LRS are highest over EAS (Figure S3c) and lowest over AUS (Figure S3g).

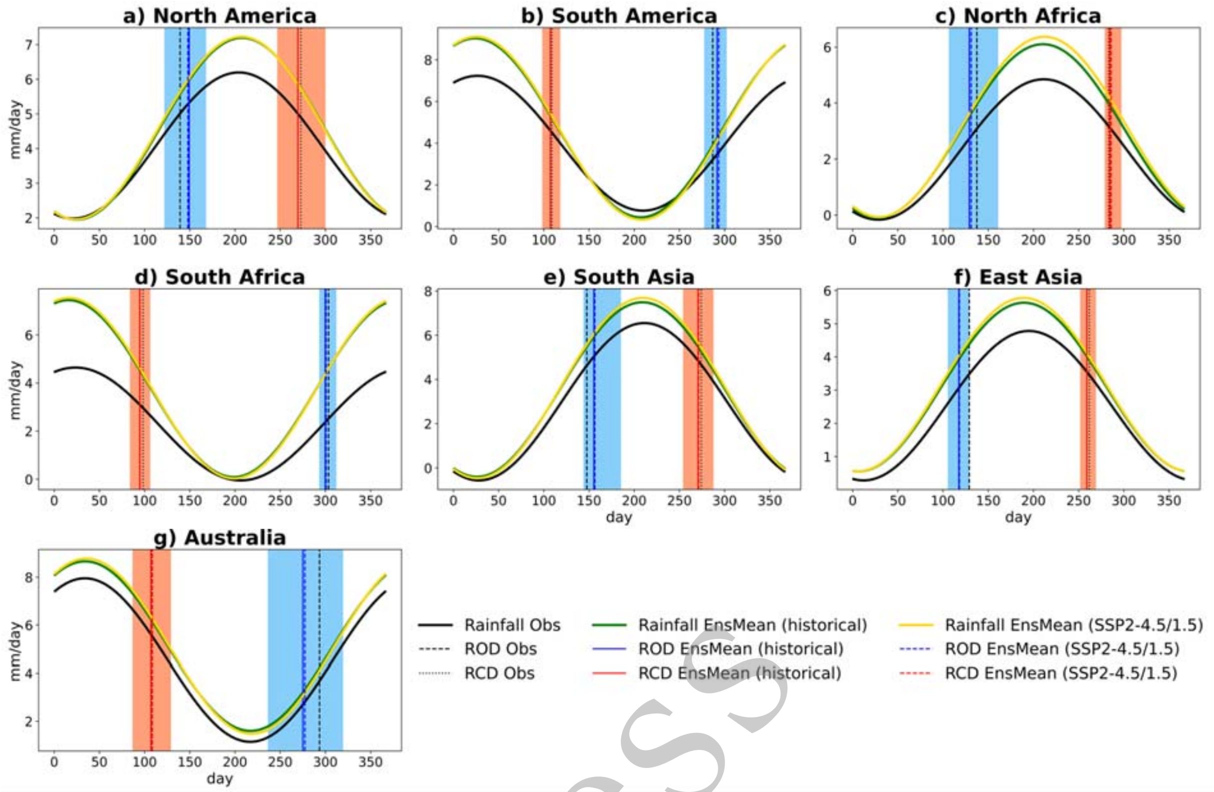


***Figure 4:*** *Annual rainfall cycle from observations (1995-2014, CPC: black line), CMIP6 EnsMean for the historical period (1995-2014: green line), and future projections under SSP2–4.5 at 1.5°C GWL (yellow line). Vertical dashed and dotted black lines indicate observed rainfall onset and cessation dates, while solid blue and red lines represent the CMIP6 historical EnsMean for these dates. Projected onset and cessation dates are shown with dashed blue and red lines, respectively, with light shading in corresponding colors representing model spread. The annual cycles are smoothed representations of the long-term daily means, derived using the first harmonic of Fourier analysis.*

Figures S4 and 6 explore the effect of an additional 0.5°C global warming climate on RODs, RCDs, and LRS over GLM regions under the Paris Agreement's proposed warming level of 1.5°C (COP21, 2015). The additional effects resulting from 2.0°C warming lead to further delay in RODs over NAF, SAF, SAS, and SAM, while earlier RODs are projected over AUS (Figure S4a, d). Over NAF (SAM), the delay is more substantial under SSP2–4.5 (SSP5–8.5) compared to SSP5–8.5 (SSP2–4.5). However, limiting the warming to below 1.5°C rather than 2.0°C will lead to positive avoided impacts on RODs in most GLM regions ,such as SAS (18%) and SAM (41%) under the SSP2–4.5 and SSP5–8.5 scenarios, respectively (Figure 6a,b). In contrast, the increase in warming from 1.5°C to 2.0°C further advances RODs by more than 6 days over AUS under the SSP5–8.5 scenario (Figure S4d). For the projected RCDs under SSP2–4.5, additional warming above 1.5°C causes a slight delay of about 2 days over NAF, while a more pronounced delay of about 4 days is projected under SSP5–8.5 (Figure S4b, e). The effect of an additional 0.5°C global warming will advance (delay) RCDs by approximately 6 days (5 days) over the western part of SAS under SSP2–4.5 (SSP5–8.5) (Figure S4c, f). Under a warmer climate, LRS is projected to be longer by about 5 days over SAS for SSP2–4.5 compared to SSP5–8.5. In both scenarios, a further decrease in LRS is projected over SAM and SAF with model consensus, and the shortest LRS is expected under the SSP5–8.5 scenario (Figure S4c, f). Limiting the warming to below 1.5°C rather than 2.0°C will avoid 34% of the impact on the projected LRS in SAF under SSP2–4.5 (Figure 6a,b). These findings suggest that a warming climate leads to a reduced likelihood of LRS, which could result in dry conditions over regions such as SAM and SAF.

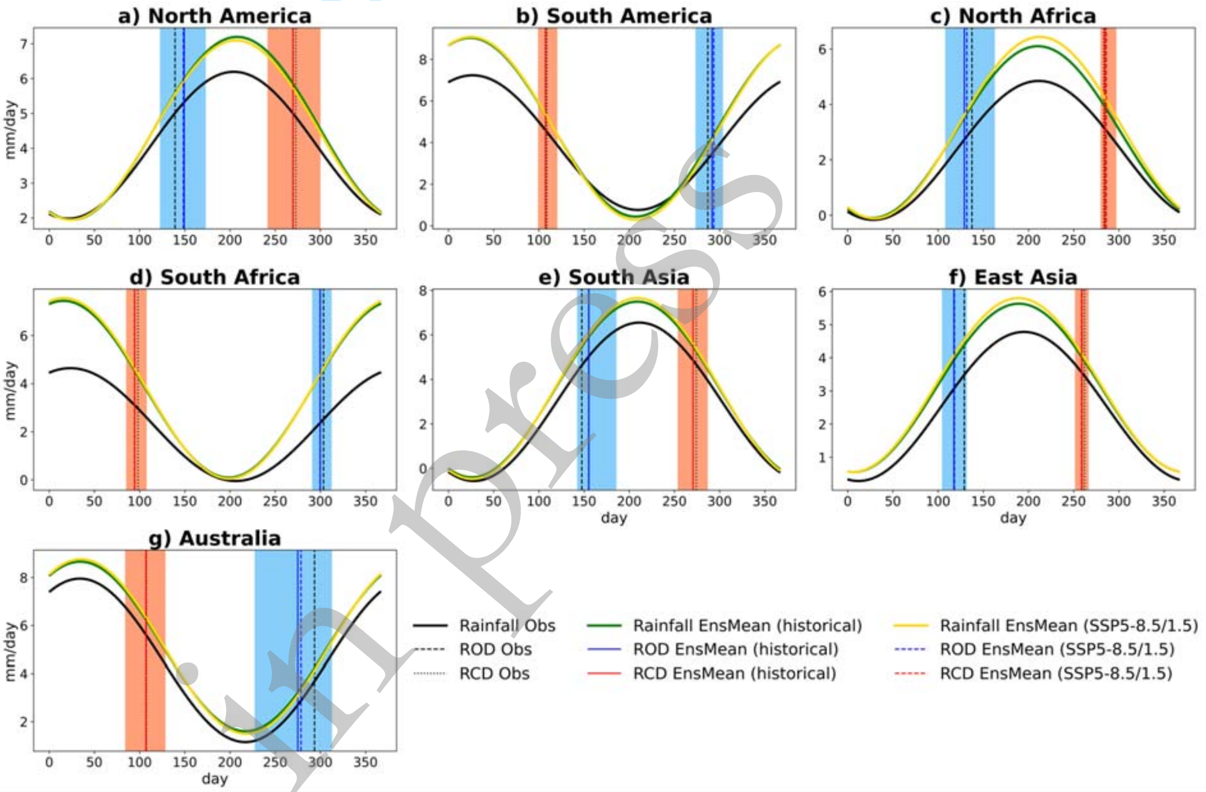


***Figure 5:*** *Annual rainfall cycle from observations (1995-2014, CPC: black line), CMIP6 EnsMean for the historical period (1995-2014: green line), and future projections under SSP5–8.5 at 1.5°C GWL (yellow line). Vertical dashed and dotted black lines indicate observed rainfall onset and cessation dates, while solid blue and red lines represent the CMIP6 historical EnsMean for these dates. Projected onset and cessation dates are shown with dashed blue and red lines, respectively, with light shading in corresponding colors representing model spread. The annual cycles are smoothed representations of the long-term daily means, derived using the first harmonic of Fourier analysis.*

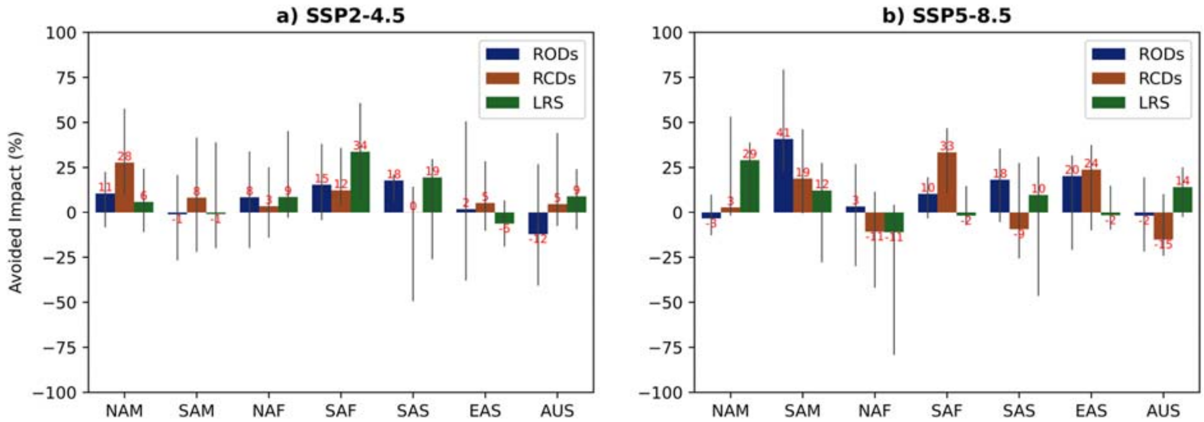


***Figure 6:*** *Avoided Impact of 0.5℃ warmer climate relative to the 1.5 ℃ warming target over GLM regions (unit: %) for rainfall onset dates (RODs), rainfall cessation dates (RCDs), and length of the rainy season (LRS) based on the CMIP6 EnsMean under the (a) SSP2–4.5 and (b) SSP5–8.5 scenarios. Projected changes are computed relative to the 1995-2014 historical period, and the error bars (vertical lines) represent 95% confidence interval based on the spread across all CMIP6 models.*

### 4.2 Future changes in precipitation characteristics within the rainy season

This section investigates how precipitation characteristics during the rainy season will be affected by 1.5°C and 2.0°C increases in global temperatures under the SSP2–4.5 and SSP5–8.5 scenarios across GLM regions. Results show a projected increase in total precipitation over WAF, SAS, and EAS (Figure 7a, d, g, j), with the increase stronger under 2.0°C GWL in both scenarios (Figure 7d, j) and higher increases (> 80 mm) over NAF (Figures 7j and 8a). The projected increase in precipitation over NAF agrees with findings from Almazroui et al. (2020) and Dosio et al. (2021). The model consensus observed over NAF in both scenarios and at both GWLs (Figure 7a, d, g, j) further indicates the robustness of the change in that region. The projected rise in precipitation could be linked to greater surface evaporation and intensified convergence of atmospheric moisture, as reported by Akinsanola and Zhou (2019). Conversely, although less robust, a projected decrease in total precipitation is observed over SAM, as also highlighted by Hodnebrog et al. (2021) and Almazroui et al. (2021). The decrease reaches -30 mm under SSP5–8.5 (Figure 7g, j). For both global warming levels, total precipitation is projected to increase under SSP2–4.5 and decrease under SSP5–8.5 in NAM (Figures 7a, d, g, j, and 8a). However, that region has large model uncertainties at 2.0°C GWL under the SSP5–8.5 scenario (Figure 8a). For the projected amount of rainfall per day, an increase is expected in all regions (Figure 7b, e, h, k). The projected increase is stronger at 2.0°C GWL in both scenarios, with the highest (> 0.6 mm/day) and more robust increase projected over NAF under SSP5–8.5 (Figure 7k). Conversely, the projected number of rainy days is expected to decrease in most monsoon regions (Figure 7c, f, i, l). The highest decrease is expected over SAM and SAF and is more pronounced (> 10 days) at 2.0°C GWL in both scenarios (Figure 7f, l), with high model consensus. However, large uncertainties exist over SAM at 2.0°C GWL under the SSP5–8.5 scenario (Figure 8c). Notably, NAF exhibits the highest increase in the projected number of rainy days, reaching up to 8 days under the SSP5–8.5 scenario at 2.0°C GWL.

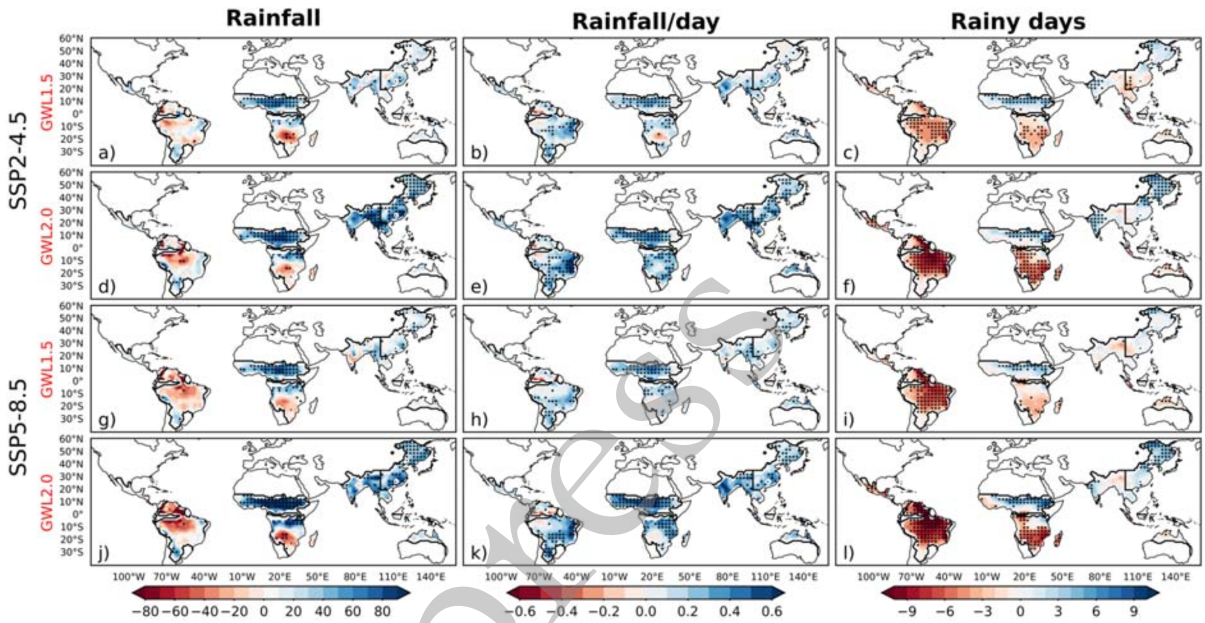


*__Figure 7:__ Future changes in total rainfall during the rainy season (mm), daily rainfall amounts (mm/day), and number of rainy days (days) across GLM regions relative to the 1995-2014 period for the CMIP6 EnsMean under the SSP2–4.5 and SSP5–8.5 scenarios at different GWLs. (a–c) SSP2–4.5 under 1.5ºC, (d–f) SSP2–4.5 under 2.0°C, (g–i) SSP5–8.5 under 1.5°C, and (j–l) SSP5–8.5 under 2.0°C. Stippling marks areas where at least 70% of the models concur on the direction of change in EnsMean.*

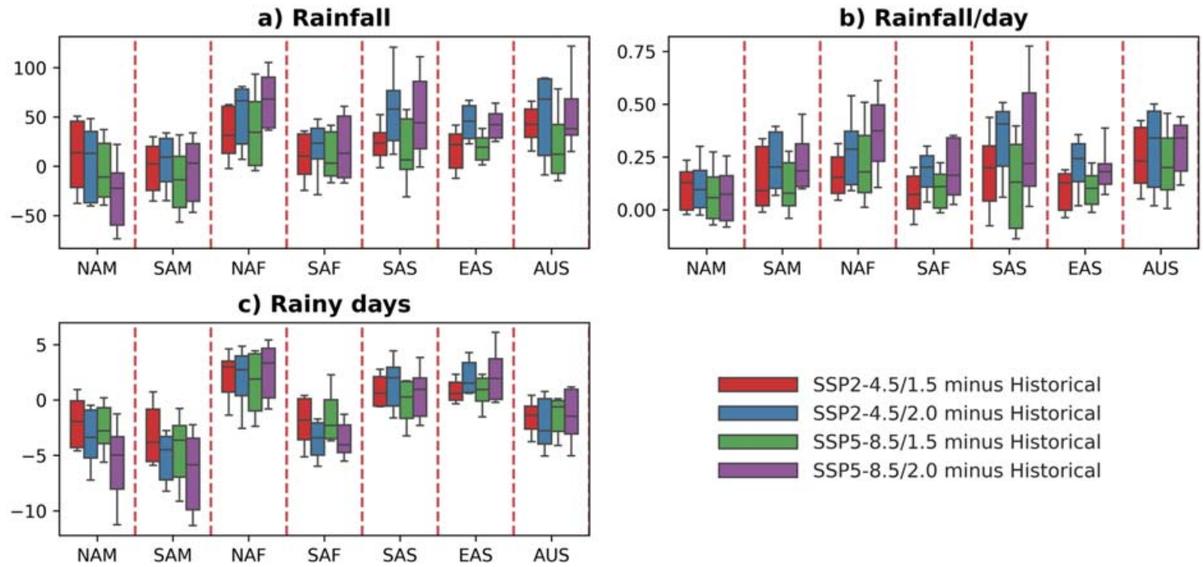


***Figure 8: :*** *Projected changes in the area averaged: (a) the total rainfall during the rainy season (mm), (b) daily rainfall amounts (mm/.day−1), and (c) the number of rainy days (days) under the SSP2–4.5 and SSP5–8.5 scenarios at various GWLs compared to the period 1995-2014 across different monsoon regions. Box-and-whisker plots illustrate the 10th, 25th, 50th, 75th, and 90th percentiles.*

Figure 9 explores the relationship between changes in total rainy season rainfall (TRSR) and changes in RODs as well as RCDs. While results vary across regions, the correlation between TRSR and RCDs is generally stronger. In SAF, under SSP2–4.5 at 1.5°C, the correlation between TRSR and RCDs reaches 0.59. Figure S5 also illustrates the statistical relationships between TRSR and the rainfall per rainy day (RPRD), as well as the relationships between TRSR and the number of rainy days (NORD) across the 16 CMIP6 models. TRSR generally exhibits a stronger correlation with RPRD across all regions at both global warming levels and under both scenarios, with the highest correlation coefficients observed in EAS, reaching up to 0.95 at a 1.5°C global warming level under the SSP2–4.5 scenario (Figure S5). This suggests that, in many regions, the rise in RPRD might have a greater impact on TRSR than the changes in the number of rainy days. This aligns with the findings of Piao et al. (2023) over East Asia, who reported a high correlation between TRSR and the rainfall per rainy season. However, TRSR is also closely associated with the number of rainy days over SAS, with correlation coefficient values of 0.75 at 2.0°C GWL under SSP2–4.5 and 0.75 at 1.5°C GWL under SSP5–8.5 (Figure S5).

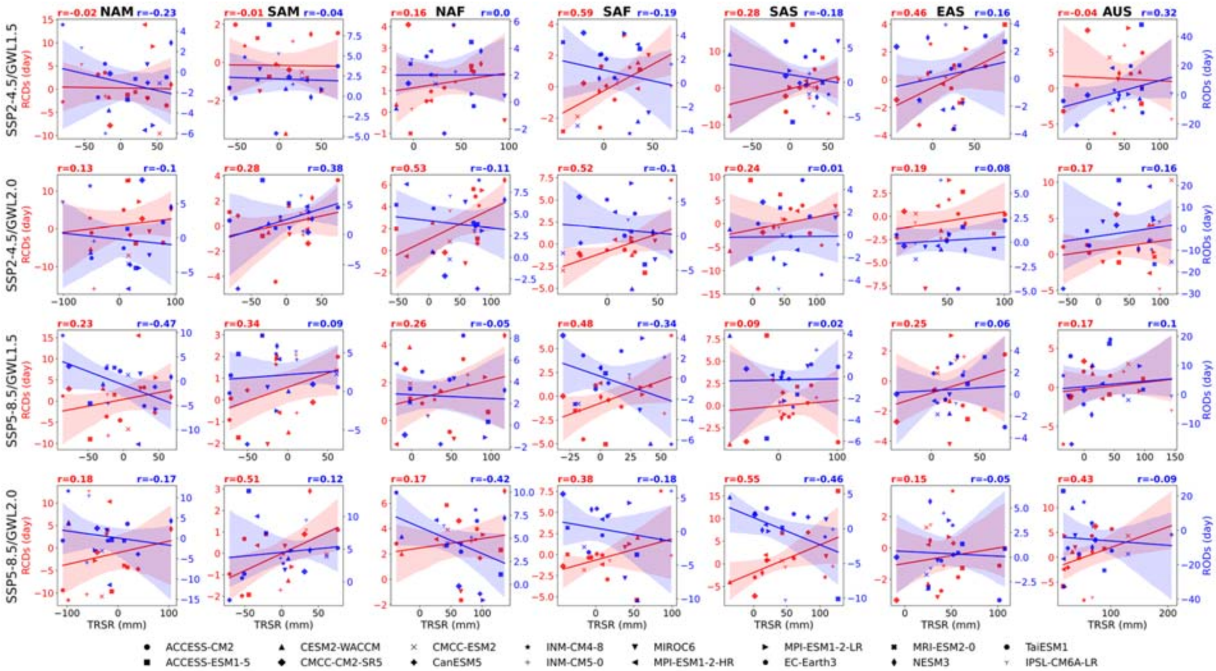


***Figure 9:*** *Scatterplots and correlation coefficients showing the relationship between changes in total rainy season rainfall (TRSR; mm) and changes in rainfall onset dates (RODs; day) (blue) as well as rainfall cessation dates (RCDs; days) (red) under the SSP2–4.5 and SSP5–8.5 scenarios at various global warming levels (GWLs) relative to the period 1995-2014 for each monsoon region across the 16 CMIP6 ensemble members. Shading indicates 95% confidence intervals.*

From 1.5°C to 2.0°C GWL, under both scenarios, there is a significant rise in TRSR and RPRD across most areas (Figures 10 and S6). Over NAF (SAS), TRSR increases by more than 30 mm under SSP5–8.5 (SSP2–4.5), while the increase is less significant under SSP2–4.5 (SSP5–8.5) (Figure 10a,d). For corresponding changes in RPRD, the increase is also more significant under SSP5–8.5 scenario in most regions, with the largest increase (>0.4 mm/day) observed west of the SAS region (Figure 10b,e). However, for both TRSR and RPRD, the impact of 2.0°C over 1.5°C generally shows larger uncertainties under SSP5–8.5 scenario (Figure S6a,b). With additional warming of 0.5°C, rainy days decreases in all regions except SAS and EAS under SSP2–4.5 scenario (Figure 10c,f). The highest decrease of about 5 days is observed over SAM. Conversely, NAF and AUS exhibit an increase in the number of rainy days under SSP5–8.5 scenario.

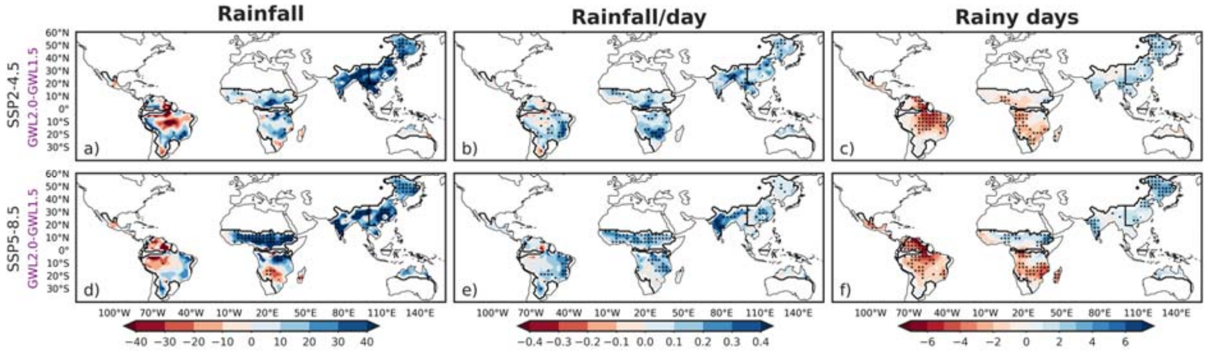


***Figure 10:*** *Projected changes in total rainfall during the rainy season (mm), the daily rainfall rate (mm/day), and the number of rainy days (days) across GLM regions relative to the 1995-2014 period for the CMIP6 EnsMean models under GWL2.0 compared to GWL1.5 for the (a–c) SSP2–4.5 and (d–f) SSP5–8.5 scenarios. Stippling marks areas where at least 70% of the models concur on the direction of change in EnsMean.*

## 5. Summary and conclusion

Exceeding the 1.5°C and 2.0°C global warming thresholds is projected to induce profound changes in global monsoon systems, with potentially devastating consequences for billions of people. This study addresses the critical question of how global land monsoon (GLM) rainfall patterns such as onset dates (RODs), cessation dates (RCDs), and the length of the rainy season (LRS) will change in the future by analyzing historical and projected precipitation data from 16 CMIP6 models under the SSP2–4.5 and SSP5–8.5 scenarios.

Our results indicate that the CMIP6 ensemble mean (EnsMean) generally captures the basic spatial features of RODs and RCDs, albeit with some biases. For example, EnsMean delays RODs by about 20–30 days over South Asia and 10–20 days over northern North America while advancing them by 20–30 days over North Africa and East Asia. EnsMean shows less bias in simulated historical RCDs than RODs, with about 10–15 days of advance over North Africa and North America. Additionally, LRS is reasonably well represented. However, there are biases in the number of days, particularly in eastern North Africa and South Asia. Individual models generally struggle more with simulating RODs than RCDs, with higher percentage bias values for RODs across most regions. Except over EAS and AUS, future changes project a delay in RODs under the SSP2–4.5 and SSP5–8.5 scenarios in most monsoon regions, particularly under the 2.0°C global warming level. The delays are more robust over regions like South America, with models showing relatively low uncertainties. Conversely, under both scenarios, RCDs are projected to advance in some regions, such as North America and Australia. The combined effects of changes in RODs and RCDs indicate a shortening of LRS over South America and South Africa, implying an intensification of dry conditions in a warming climate. Additionally, the study finds that total precipitation and the intensity of rainfall per day within the rainy season are projected to increase over most regions, particularly under the SSP5–8.5 scenario. This increase is accompanied by a decrease in rainy days, suggesting a shift toward more intense but less frequent rainfall events. These findings underscore the importance of limiting global warming to below 2.0°C to mitigate adverse impacts on precipitation patterns and the length of the rainy season.

Changes in the timing of the rainy season can have significant implications for various sectors, particularly agriculture. For instance, the projected delays in the onset of the rainy season in SAM can disrupt planting schedules, reducing crop yields. Farmers rely on predictable rainfall patterns to time their planting, and any deviation can result in crops not reaching maturity before the end of the rainy season. Also, delayed onset affects water availability for irrigation and other uses. This can strain water resources, especially in regions already facing water scarcity. The timing of rainy season cessation also carries critical implications. For example, the projected early cessation over NAM and SAF can reduce the growing season, preventing crops from reaching full maturity and reducing yields. This is particularly detrimental for crops that require longer growing periods. Also, an early end to the rainy season can increase the risk of drought, affecting agriculture and water supply for domestic and industrial use. The overall length of the rainy season, determined by the onset and cessation dates, has profound implications. As projected in most GLM regions, a shortened rainy season can lead to insufficient crop water, reducing yields and potentially leading to food shortages. Also, changes in the length of the rainy season can alter the balance between flood and drought periods. However, in North Africa, the projected increase in the total rainy season rainfall, along with the rainfall per rainy day, might mitigate drought risks but increase flooding incidents, damaging infrastructure, homes, and livelihoods, particularly in urban areas with poor drainage systems. Therefore, understanding the projected changes in rainfall characteristics is crucial for developing effective climate adaptation strategies. These include rainwater harvesting, improved irrigation techniques, and developing drought-resistant crop varieties.

***Acknowledgments:*** We thank the World Climate Research Programme's Working Group on Coupled Modeling for managing the CMIP initiative and express our gratitude to the climate modeling groups (as listed in Table S1) for their model outputs. We also appreciate the institution that provided the CPC observational data used in this research. Oluwafemi E. Adeyeri is supported by Australian Research Council grant number CE230100012.

**References**

Adeyeri, O. E., Zhou, W., Ndehedehe, C. E., Wang, X., Ishola, K. A., & Laux, P. (2024). Minimizing uncertainties in climate projections and water budget reveals the vulnerability of freshwater to climate change. *One Earth*, *7*(1), 72–87. https://doi.org/10.1016/j.oneear.2023.12.013

Akinsanola, A. A., & Zhou, W. (2019). Ensemble-based CMIP5 simulations of West African summer monsoon rainfall: Current climate and future changes. *Theoretical and Applied Climatology*, *136*(3–4), 1021–1031. https://doi.org/10.1007/s00704-018-2516-3

Akinsanola, A. A., & Zhou, W. (2020). Understanding the Variability of West African Summer Monsoon Rainfall: Contrasting Tropospheric Features and Monsoon Index. *Atmosphere*, *11*(3), 309. https://doi.org/10.3390/atmos11030309

Akinsanola, A. A., Ongoma, V., & Kooperman, G. J. (2021). Evaluation of CMIP6 models in simulating the statistics of extreme precipitation over Eastern Africa. *Atmospheric Research*, *254*, 105509. https://doi.org/10.1016/j.atmosres.2021.105509

Akinsanola, A. A., Chen, Z., Kooperman, G. J., & Bobde, V. (2024). Robust future intensification of winter precipitation over the United States. *Npj Climate and Atmospheric Science*, *7*(1). https://doi.org/10.1038/s41612-024-00761-8

Akinsanola, A. A., Adebiyi, A. A., Bobde, V., Adeyeri, O. E., Tamoffo, A. T., & Danso, D. K. (2025). Projected changes in African easterly wave activity due to climate change. *Communications Earth & Environment*, *6*(1). https://doi.org/10.1038/s43247-024-01981-9

Almazroui, M., Saeed, F., Saeed, S., Islam, M. N., Ismail, M., Klutse, N. A. B., & Siddiqui, M. H. (2020). Projected Change in Temperature and Precipitation Over Africa from CMIP6.

*Earth Systems and Environment*, *4*(3), 455–475. https://doi.org/10.1007/s41748-020-00161-x

Almazroui, M., Ashfaq, M., Islam, M. N., Rashid, I. U., Kamil, S., Abid, M. A., O'Brien, E., Ismail, M., Reboita, M. S., Sörensson, A. A., Arias, P. A., Alves, L. M., Tippett, M. K., Saeed, S., Haarsma, R., Doblas-Reyes, F. J., Saeed, F., Kucharski, F., Nadeem, I., . . . Sylla, M. B. (2021). Assessment of CMIP6 Performance and Projected Temperature and Precipitation Changes Over South America. *Earth Systems and Environment*, *5*(2), 155–183. https://doi.org/10.1007/s41748-021-00233-6

Amekudzi, L., Yamba, E., Preko, K., Asare, E., Aryee, J., Baidu, M., & Codjoe, S. (2015). Variabilities in Rainfall Onset, Cessation and Length of Rainy Season for the Various Agro-Ecological Zones of Ghana. *Climate*, *3*(2), 416–434. https://doi.org/10.3390/cli3020416

Atiah, W. A., Muthoni, F. K., Kotu, B., Kizito, F., & Amekudzi, L. K. (2021). Trends of Rainfall Onset, Cessation, and Length of Growing Season in Northern Ghana: Comparing the Rain Gauge, Satellite, and Farmer's Perceptions. *Atmosphere*, *12*(12), 1674. https://doi.org/10.3390/atmos12121674

Ayugi, B., Dike, V., Ngoma, H., Babaousmail, H., Mumo, R., & Ongoma, V. (2021). Future Changes in Precipitation Extremes over East Africa Based on CMIP6 Models. *Water*, *13*(17), 2358. https://doi.org/10.3390/w13172358

Ayugi, B., Jiang, Z., Iyakaremye, V., Ngoma, H., Babaousmail, H., Onyutha, C., Dike, V. N., Mumo, R., & Ongoma, V. (2022). East African population exposure to precipitation extremes under 1.5 °C and 2.0 °C warming levels based on CMIP6 models. *Environmental Research Letters*, *17*(4), 044051. https://doi.org/10.1088/1748-9326/ac5d9d

Bobde, V., Akinsanola, A. A., Folorunsho, A. H., Adebiyi, A. A., & Adeyeri, O. E. (2024). Projected regional changes in mean and extreme precipitation over Africa in CMIP6 models. *Environmental Research Letters*. https://doi.org/10.1088/1748-9326/ad545c

Bombardi, R. J., Kinter, J. L., & Frauenfeld, O. W. (2019). A Global Gridded Dataset of the Characteristics of the Rainy And Dry Seasons. *Bulletin of the American Meteorological Society*, *100*(7), 1315–1328. https://doi.org/10.1175/bams-d-18-0177.1

Bombardi, R. J., & Boos, W. R. (2021). Explaining Globally Inhomogeneous Future Changes in Monsoons Using Simple Moist Energy Diagnostics. *Journal of Climate*, *34*(21), 8615–8634. https://doi.org/10.1175/jcli-d-20-1012.1

Chakraborty, A., & Singhai, P. (2021). Asymmetric response of the Indian summer monsoon to positive and negative phases of major tropical climate patterns. *Scientific Reports*, *11*(1), 22561.

Chang, M., Liu, B., Wang, B., Martinez-Villalobos, C., Ren, G., & Zhou, T. (2022). Understanding Future Increases in Precipitation Extremes in Global Land Monsoon Regions. *Journal of Climate*, *35*(6), 1839–1851. https://doi.org/10.1175/jcli-d-21-0409.1

Chen, Z., Zhou, T., Zhang, L., Chen, X., Zhang, W., & Jiang, J. (2020). Global land monsoon precipitation changes in CMIP6 projections. *Geophysical Research Letters*, *47*, e2019GL086902. https://doi.org/10.1029/2019GL086902

Cheng, Y., Wang, L., Chen, X., Zhou, T., Turner, A., & Wang, L. (2024). Constrained Projections Indicate Less Delay in Onset of Summer Monsoon over the Bay of Bengal and South China Sea. *Geophysical Research Letters*, *51*(21). https://doi.org/10.1029/2024gl110994

Cheng, Y., Wang, L., Chen, X., Zhou, T., & Turner, A. (2025). A shorter duration of the Indian summer monsoon in constrained projections. *Geophysical Research Letters*, *52*(1). https://doi.org/10.1029/2024gl112848

Collini, E. A., Berbery, E. H., Barros, V. R., & Pyle, M. E. (2008). How Does Soil Moisture Influence the Early Stages of the South American Monsoon? *Journal of Climate*, *21*(2), 195–213. https://doi.org/10.1175/2007jcli1846.1

COP21 (2015) The Paris Agreement, United Nations Framework Convention on Climate Change (UNFCCC), Paris France. https://unfccc.int/process-and-meetings/the-paris-agreement/the-paris-agreement

Daron, J., Burgin, L., Janes, T., et al (2019) Climate process chains: Examples from southern Africa. *Int J Climatol 39*, 4784–4797. https://doi.org/10.1002/joc.6106

Das, L., Akhter, J., Dutta, M., & Meher, J. K. (2015). Ensemble-based CMIP5 simulations of monsoon rainfall and temperature changes over South Asia. *Chall. Agro-Environ. Res. Monsoon Asia*, *6*, 41-60.

Das, S., Kamruzzaman, M., & Islam, A. R. M. T. (2022). Assessment of characteristic changes of regional estimation of extreme rainfall under climate change: A case study in a tropical monsoon region with the climate projections from CMIP6 model. *Journal of Hydrology*, *610*, 128002. https://doi.org/10.1016/j.jhydrol.2022.128002

Dash, S. K., Jenamani, R. K., Kalsi, S. R., & Panda, S. K. (2007). Some evidence of climate change in twentieth-century India. *Climatic Change*, *85*(3-4), 299-321.

Deng, K., S. Yang, M. Ting, Y. Tan, and S. He, 2018: Global monsoon precipitation: Trends, leading modes, and associated drought and heat wave in the Northern Hemisphere. *J. Climate, 31*, 6947–6966, https://doi.org/10.1175/JCLI-D-17-0569.1.

Donat, M. G., Lowry, A. L., Alexander, L. V., O'Gorman, P. A., & Maher, N. (2016). More extreme precipitation in the world's dry and wet regions. *Nature Climate Change, 6*(5), 508-513.

Dosio, A., Jury, M. W., Almazroui, M., Ashfaq, M., Diallo, I., Engelbrecht, F. A., Klutse, N. a. B., Lennard, C., Pinto, I., Sylla, M. B., & Tamoffo, A. T. (2021). Projected future daily characteristics of African precipitation based on global (CMIP5, CMIP6) and regional (CORDEX, CORDEX-CORE) climate models. *Climate Dynamics*, *57*(11–12), 3135–3158. https://doi.org/10.1007/s00382-021-05859-w

Dunning, C. M., Black, E., & Allan, R. P. (2018). Later Wet Seasons with More Intense Rainfall over Africa under Future Climate Change. *Journal of Climate*, *31*(23), 9719–9738. https://doi.org/10.1175/jcli-d-18-0102.1

Dwyer, J. G., Biasutti, M., & Sobel, A. H. (2014). The Effect of Greenhouse Gas–Induced Changes in SST on the Annual Cycle of Zonal Mean Tropical Precipitation. *Journal of Climate*, *27*(12), 4544–4565. https://doi.org/10.1175/jcli-d-13-00216.1

Eyring, V., Bony, S., Meehl, G. A., A, C., Senior, Stevens, B., Stouffer, R. J., & Taylor, K. E. (2016). Overview of the Coupled Model Intercomparison Project Phase 6 (CMIP6) experimental design and organization. *Geoscientific Model Development*, *9*(5), 1937–1958. https://doi.org/10.5194/gmd-9-1937-2016

Faye, A., & Akinsanola, A. A. (2021). Evaluation of extreme precipitation indices over West Africa in CMIP6 models. Climate Dynamics, 58(3–4), 925–939. https://doi.org/10.1007/s00382-021-05942-2

Gadgil, S., & Gadgil, S. (2006). The Indian monsoon, GDP and agriculture. *Economic and Political Weekly*, 4887-4895.

Ha, K.-J., Moon, S., Timmermann, A., & Kim, D. (2020). Future changes of summer monsoon characteristics and evaporative demand over Asia in CMIP6 simulations. *Geophysical Research Letters, 47*, e2020GL087492. https://doi.org/10.1029/2020GL087492

Hariadi, M. H., Van Der Schrier, G., Steeneveld, G., Sopaheluwakan, A., Tank, A. K., Roberts, M. J., Moine, M., Bellucci, A., Senan, R., Tourigny, E., & Putrasahan, D. (2021). Evaluation of onset, cessation and seasonal precipitation of the Southeast Asia rainy season in CMIP5 regional climate models and HighResMIP global climate models. *International Journal of Climatology*, *42*(5), 3007–3024. https://doi.org/10.1002/joc.7404

Hauser, M., Engelbrecht, F., & Fischer, E. M. (2021). Transient global warming levels for CMIP5 and CMIP6. https://doi.org/10.5281/zenodo.3591806

Hodnebrog, Ø., Steensen, B. M., Marelle, L., Alterskjær, K., Dalsøren, S. B., & Myhre, G. (2021). Understanding model diversity in future precipitation projections for South America. *Climate Dynamics*, *58*(5–6), 1329–1347. https://doi.org/10.1007/s00382-021-05964-w

Intergovernmental Panel on Climate Change (IPCC) (2021). Climate Change 2021: The Physical Science Basis. Contribution of Working Group I to the Sixth Assessment Report of the Intergovernmental Panel on Climate Change. Cambridge University Press. https://www.ipcc.ch/report/ar6/wg1/

Jin, C., Wang, B., & Liu, J. (2020). Future Changes and Controlling Factors of the Eight Regional Monsoons Projected by CMIP6 Models. *Journal of Climate*, *33*(21), 9307–9326. https://doi.org/10.1175/jcli-d-20-0236.1

Jones, C., & Carvalho, L. M. V. (2013). Climate change in the South American monsoon system: Present climate and CMIP5 projections. *Journal of Climate, 26*(17), 6660-6678. https://doi.org/10.1175/JCLI-D-12-00412.1

Khadka, D., Babel, M. S., Abatan, A. A., & Collins, M. (2021). An evaluation of CMIP5 and CMIP6 climate models in simulating summer rainfall in the Southeast Asian monsoon domain. *International Journal of Climatology*, *42*(2), 1181-1202.

Kitoh, A., Endo, H., Krishna Kumar, K., Cavalcanti, I. F. A., Goswami, P., & Zhou, T. (2013). Monsoons in a changing world: A regional perspective in a global context. *Journal of Geophysical Research: Atmospheres, 118*(6), 3053-3065. https://doi.org/10.1002/jgrd.50258

Kumi, N., & Abiodun, B. J. (2018). Corrigendum: Potential impacts of 1.5 °C and 2 °C global warming on rainfall onset, cessation and length of rainy season in West Africa (2018 Environ. Res. Lett. 13 055009). *Environmental Research Letters*, *13*(8), 089502. https://doi.org/10.1088/1748-9326/aad5c6

Lee, J.-Y., & Wang, B. (2014). Future change of global monsoon in the CMIP5. *Climate Dynamics, 42*(1-2), 101-119. https://doi.org/10.1007/s00382-012-1564-0

Lehmann, J., Coumou, D. and Frieler, K. (2015) Increased record-breaking precipitation events under global warming. *Climatic Change, 132*(4), 501–515.

https://doi.org/10.1007/s10584-015-1434-y.

Liebmann, B., & Marengo, J. (2001). Interannual variability of the rainy season and rainfall in the Brazilian Amazon basin. *Journal of Climate*, *14*(22), 4308–4318. https://doi.org/10.1175/1520-0442(2001)014

Liu, F., Wang, B., Ouyang, Y., Wang, H., Qiao, S., Chen, G., & Dong, W. (2022). Intraseasonal variability of global land monsoon precipitation and its recent trend. *Npj Climate and Atmospheric Science*, *5*(1). https://doi.org/10.1038/s41612-022-00253-7

Majdi, F., Hosseini, S. A., Karbalaee, A., Kaseri, M., & Marjanian, S. (2022). Future projection of precipitation and temperature changes in the Middle East and North Africa (MENA) region based on CMIP6. *Theoretical and Applied Climatology*, *147*(3–4), 1249–1262. https://doi.org/10.1007/s00704-021-03916-2

Menon, A., Levermann, A., Schewe, J., Lehmann, J., & Frieler, K. (2013). Consistent increase in Indian monsoon rainfall and its variability across CMIP-5 models. *Earth System Dynamics*, *4*(2), 287–300. https://doi.org/10.5194/esd-4-287-2013

Mishra, A., & Liu, S. C. (2014). Changes in precipitation pattern and risk of drought over India in the context of global warming. *Journal of Geophysical Research Atmospheres*, *119*(13), 7833–7841. https://doi.org/10.1002/2014jd021471

Mishra, A.K. (2015) A study on the occurrence of flood events over Jammu and Kashmir during September 2014 using satellite remote sensing. *Natural Hazards, 78*(2), 1463–1467. https://doi.org/10.1007/s11069-015-1768-9.

Moon, S., and K.-J. Ha, 2020: Future changes in monsoon duration and precipitation using CMIP6. *npj Climate Atmos. Sci., 3*, 45, https://doi.org/10.1038/s41612-020-00151-w.

Mugalavai, E. M., Kipkorir, E. C., Raes, D., & Rao, M. S. (2008). Analysis of rainfall onset, cessation and length of growing season for western Kenya. *Agricultural and Forest Meteorology*, *148*(6–7), 1123–1135. https://doi.org/10.1016/j.agrformet.2008.02.013

Mwangi, E., MacLeod, D., Kniveton, D., & Todd, M. C. (2024). Variability of rainy season onsets over East Africa. *International Journal of Climatology*. https://doi.org/10.1002/joc.8528

Ni, Y., & Hsu, P. (2018). Inter-annual variability of global monsoon precipitation in present-day and future warming scenarios based on 33 Coupled Model Intercomparison Project Phase 5 models. *International Journal of Climatology*, *38*(13), 4875–4890. https://doi.org/10.1002/joc.5704

Nicholson, S. E. (2018). The ITCZ and the seasonal cycle over equatorial Africa. *Science*, 361(6406), 1117-1120.

Omay, P. O., Muthama, N. J., Oludhe, C., Kinama, J. M., Artan, G., & Atheru, Z. (2023). Changes and variability in rainfall onset, cessation, and length of rainy season in the IGAD region of Eastern Africa. *Theoretical and Applied Climatology*, *152*(1–2), 871–893. https://doi.org/10.1007/s00704-023-04433-0

Omondi, P., Awange, J. L., Forootan, E., Otieno, V. O., Motlagh, M. S., & Saleem, A. (2014). Changes in temperature and precipitation extremes over the Greater Horn of Africa region from 1961 to 2010. *International Journal of Climatology, 34*(4), 1262-1277. https://doi.org/10.1002/joc.3763

Omotosho, J. B., Balogun, A. A., & Ogunjobi, K. (2000). Predicting monthly and seasonal rainfall, onset and cessation of the rainy season in West Africa using only surface data *Int. J. Climatology, 20,* 865–80.

O'Neill, B. C., Kriegler, E., Ebi, K. L., Kemp-Benedict, E., Riahi, K., Rothman, D. S., Van Ruijven, B. J., Van Vuuren, D. P., Birkmann, J., Kok, K., Levy, M., & Solecki, W. (2017). The roads ahead: Narratives for shared socioeconomic pathways describing world futures in the 21st century. *Global Environmental Change*, *42*, 169–180. https://doi.org/10.1016/j.gloenvcha.2015.01.004

Piao, J., Chen, W., Kim, J. S., Zhou, W., Chen, S., Hu, P., & Lan, X. (2023). Future changes in rainy season characteristics over East China under continuous warming. *Climatic Change*, *176*(9). https://doi.org/10.1007/s10584-023-03598-x

Preethi, B., Mujumdar, M., Kripalani, R.H., Prabhu, A. and Krishnan, R. (2017) Recent trends and tele-connections among South and East Asian summer monsoons in a warming environment. *Climate Dynamics, 48*(7–8), 2489–2505.

Sabeerali, C. T., & Ajayamohan, R. S. (2018). On the shortening of Indian summer monsoon season in a warming scenario. *Climate Dynamics*, *50*(5–6), 1609–1624. https://doi.org/10.1007/s00382-017-3709-7

Seager, R., Naik, N., & Vecchi, G. A. (2010). Thermodynamic and dynamic mechanisms for large-scale changes in the hydrological cycle in response to global warming. *Journal of Climate, 23*(17), 4651–4668. https://doi.org/10.1175/2010jcli3655.1

Seth, A., A. Giannini, M. Rojas, S. A. Rauscher, S. Bordoni, D. Singh, and S. J. Camargo, (2019). Monsoon responses to climate changes-Connecting past, present and future. *Curr. Climate Change Rep., 5*, 63–79, https://doi.org/10.1007/s40641-019-00125-y.

Sharmila, S., Joseph, S., Sahai, A., Abhilash, S., & Chattopadhyay, R. (2015). Future projection of Indian summer monsoon variability under climate change scenario: An assessment from CMIP5 climate models. *Global and Planetary Change*, *124*, 62–78. https://doi.org/10.1016/j.gloplacha.2014.11.004

Singhai, P., Chakraborty, A., Rajendran, K., & Surendran, S. (2023). Why is the Indian summer monsoon in CFSv2 hypersensitive to moisture exchange with the Pacific Ocean? *Climate Dynamics*, *61*(9), 4515-4531.

Sylla, M. B., Diallo, I., & Pal, J. S. (2013). West African monsoon in state-of-the-science regional climate models Climate Variability-Regional and Thematic Patterns (London: InTech) (https://doi.org/10.5772/55140)

Sylla, M. B., Nikiema, P. M., Gibba, P., Kebe, I., & Klutse, N. A. B. (2016). Climate change over West Africa: Recent trends and future projections. *Adaptation to Climate Change and Variability in Rural West Africa*, 25-40. https://doi.org/10.1007/978-3-319-31499-0_3

Taguela, T. N., Vondou, D. A., Moufouma-Okia, W., Fotso-Nguemo, T. C., Pokam, W. M., Tanessong, R. S., Yepdo, Z. D., Haensler, A., Longandjo, G. N., Bell, J. P., Takong, R. R., & Djiotang Tchotchou, L. A. (2020). CORDEX Multi-RCM Hindcast Over Central Africa: Evaluation Within Observational Uncertainty. *Journal of Geophysical Research: Atmospheres*, *125*(5), e2019JD031607. https://doi.org/10.1029/2019JD031607

Taguela, T. N., Akinsanola, A. A., Bobde, V., Raji, I., Adeyeri, O. E., & Adebiyi, A. A. (2025). Precipitation distribution over Africa: observations and modeling. In *Elsevier eBooks* (pp. 121–146). https://doi.org/10.1016/b978-0-44-314050-1.00009-8

Turner, A. G., & Annamalai, H. (2012). Climate change and the South Asian summer monsoon. *Nature Climate Change*, *2*(8), 587-595.

Vera, C., B. Liebmann, & P. González, (2006). Climate change scenarios for seasonal precipitation in South America from IPCC-AR4 models. *Geophys. Res. Lett., 33*, L13707, https://doi.org/10.1029/2006GL025759.

Wainwright, C. M., Black, E., & Allan, R. P. (2021). Future Changes in Wet and Dry Season Characteristics in CMIP5 and CMIP6 simulations. *Journal of Hydrometeorology*. https://doi.org/10.1175/jhm-d-21-0017.1

Wang, B., & Ding, Q. (2008). Global monsoon: Dominant mode of annual variation in the tropics. *Dynamics of Atmospheres and Oceans,* *44*(3–4), 165–183. https://doi.org/10.1016/j.dynatmoce.2007.05.002

Wang, B., Liu, J., Kim, H.-J., Webster, P. J., & Yim, S.-Y. (2012). Recent change of the global monsoon precipitation (1979–2008). *Climate Dynamics, 39*(5), 1123–1135. https://doi.org/10.1007/s00382-011-1266-z

Wang, B., Li, J., & He, Q. (2017). Variable and robust East Asian monsoon rainfall response to global warming. *Nature Climate Change, 10*(6), 546-550. https://doi.org/10.1038/s41558-020-0748-8

Wang, B., Jin, C., & Liu, J. (2020). Understanding Future Change of Global Monsoons Projected by CMIP6 Models. *Journal of Climate*, *33*(15), 6471–6489. https://doi.org/10.1175/jcli-d-19-0993.1

Wang, L., Cheng, Y., Chen, X., & Zhou, T. (2024). Projected Changes in the Onset of the Summer Monsoon over the South Asian Marginal Seas Modulated by Intraseasonal Oscillation. *Journal of Climate, 37*(3), 821–835. https://doi.org/10.1175/jcli-d-23-0257.1

Wang, P. X., Wang, B., Cheng, H., Fasullo, J., Guo, Z., Kiefer, T., & Liu, Z. (2017). The global monsoon across time scales: Mechanisms and outstanding issues. *Earth-science Reviews*, *174*, 84–121. https://doi.org/10.1016/j.earscirev.2017.07.006

Xie, P., M. Chen, and W. Shi, (2010): CPC Unified gauge-based analysis of global daily precipitation. *24th Conf. on Hydrology*, Atlanta, GA, Amer. Meteor. Soc., 2.3A. [Available online at https://ams.confex.com/ams/90annual/webprogram/Paper163676.html.]

Yao, J., Chen, Y., Chen, J., Zhao, Y., Tuoliewubieke, D., Li, J., Yang, L., & Mao, W. (2021). Intensification of extreme precipitation in arid Central Asia. *Journal of Hydrology*, *598*, 125760. https://doi.org/10.1016/j.jhydrol.2020.125760

Yim, S. Y., Wang, B., Liu, J., & Wu, Z. (2014). A comparison of regional monsoon variability using monsoon indices. *Climate Dynamics*, *43*(5–6), 1423–1437. https://doi.org/10.1007/s00382-013-1956-9

Zhang, W., Li, H., Jin, F. F., Stuecker, M. F., & Turner, A. G. (2018). A new understanding of El Niño's impact over East Asia: Dominance of the ENSO combination mode. *Journal of Climate*, *31*(19), 7967-7985.

Zhang, W., & Zhou, T. (2019a). Increasing impacts from extreme precipitation on population over China with global warming. *Science Bulletin, 65*(3), 243–252. https://doi.org/10.1016/j.scib.2019.12.002

Zhang, W., & Zhou, T. (2019b). Significant increases in extreme precipitation and the associations with global warming over the global land monsoon regions. *Journal of Climate, 32*(24), 8465–8488. https://doi.org/10.1175/JCLI-D-18-0662.1

Zhang, X., Alexander, L., Hegerl, G. C., Jones, P., Tank, A. K., Peterson, T. C., Trewin, B., & Zwiers, F. W. (2011). Indices for monitoring changes in extremes based on daily temperature and precipitation data. *Wiley Interdisciplinary Reviews. Climate Change*, *2*(6), 851–870. https://doi.org/10.1002/wcc.147

Zhou, T., Lu, J., Zhang, W., & Chen, Z. (2020). The sources of uncertainty in the projection of global land monsoon precipitation. *Geophysical Research Letters, 47*, e2020GL088415. https://doi.org/10.1029/2020GL0884150

# Supplementary Material

## Contents of this file

Figures S1 to S6

Table S1

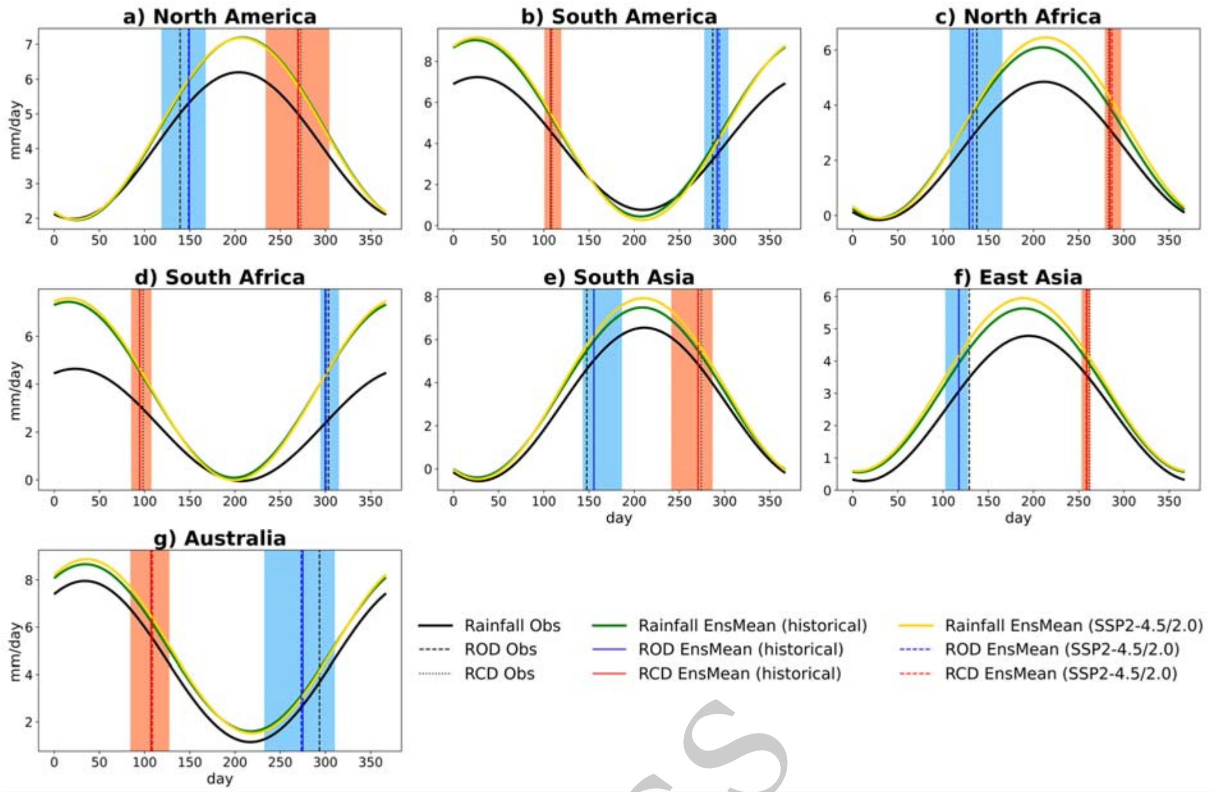


**Figure S1:** *Annual rainfall cycle from observations (1995-2014, CPC: black line), CMIP6 EnsMean for the historical period (1995-2014: green line), and future projections under SSP2–4.5 at 2.0°C GWL (yellow line). Vertical dashed and dotted black lines indicate observed rainfall onset and cessation dates, while solid blue and red lines represent the CMIP6 historical EnsMean for these dates. Projected onset and cessation dates are shown with dashed blue and red lines, respectively, with light shading in corresponding colors representing model spread. The annual cycles are smoothed representations of the long-term daily means, derived using the first harmonic of Fourier analysis.*

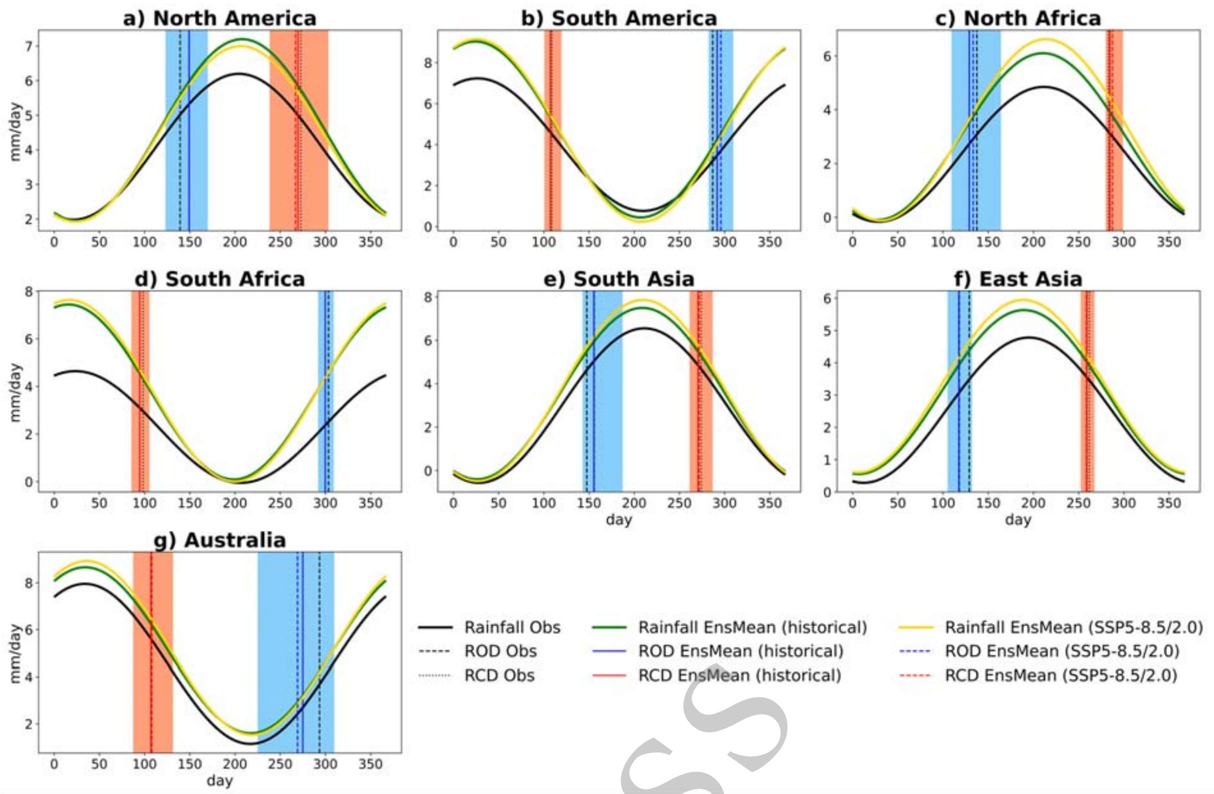


**Figure S2:** *Same as Figure S1 for SSP5–8.5 at 2.0°C*

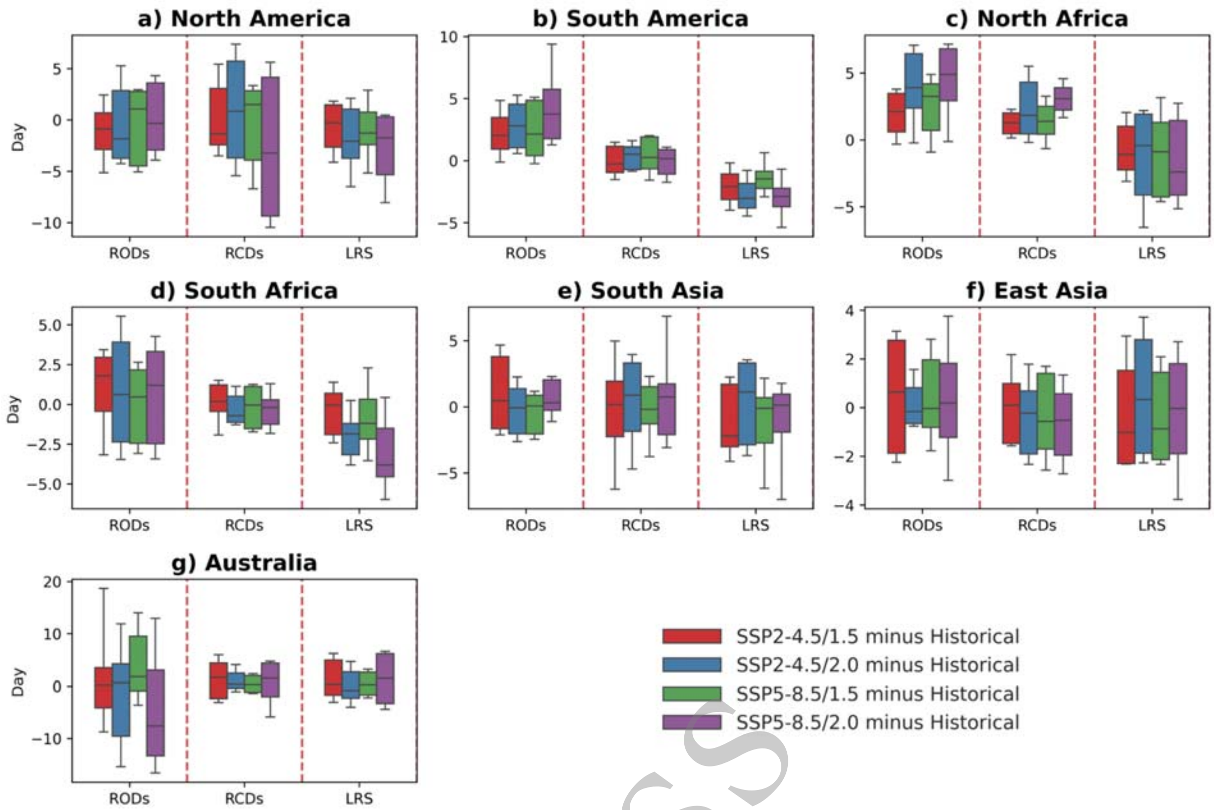


**Figure S3**: *Projected changes in the area-average rainfall onset dates (RODs) and cessation dates (RCDs), as well as the length of the rainy season (LRS), under SSP2–4.5 and SSP5–8.5 scenarios at various GWLs compared to the historical period (1995-2014) across different monsoon regions. Box-and-whisker plots illustrate the 10th, 25th, 50th, 75th, and 90th percentiles.*

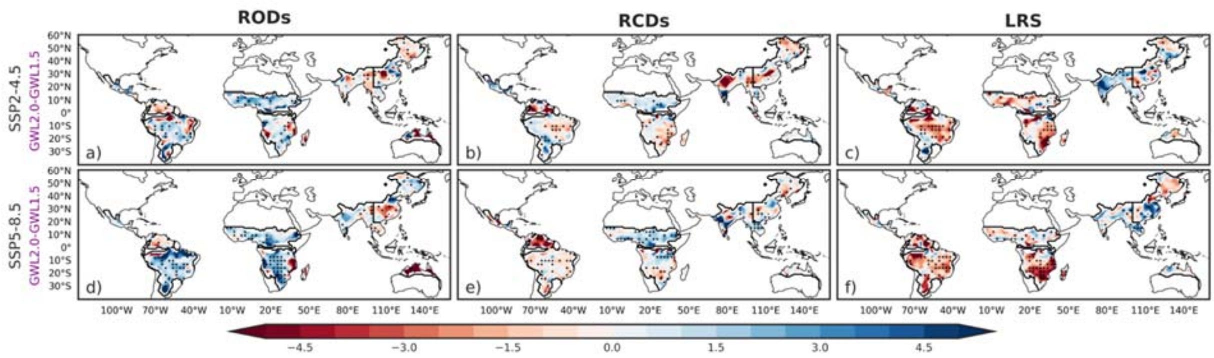


**Figure S4:** *Projected changes in the rainfall onset dates (RODs) and cessation dates (RCDs), as well as the length of the rainy season (LRS), over GLM regions relative to the 1995-2014 period for the CMIP6 EnsMean at GWL2.0 compared to GWL1.5 under (a–c) SSP2–4.5 scenario and (d–f) SSP5–8.5 scenario. Stippling marks areas where at least 70% of the models agree on the direction of change in the EnsMean.*

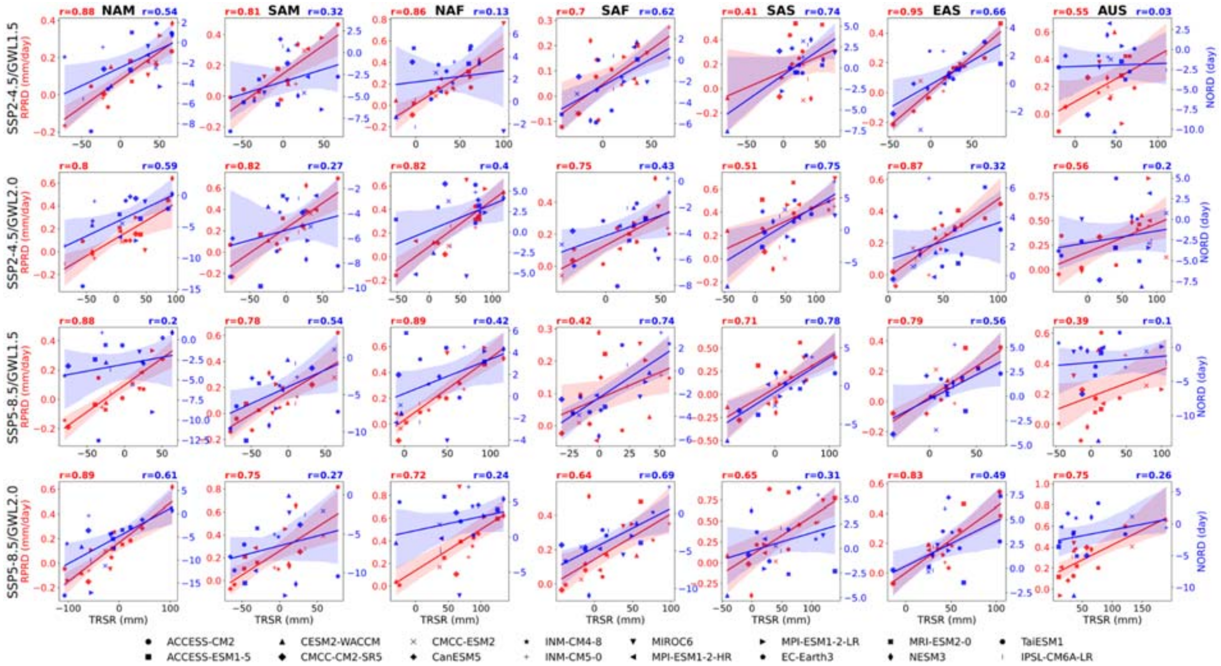


***Figure S5:*** *Scatterplots and correlation coefficients showing the relationship between changes in total rainy season rainfall (TRSR; mm) and changes in rainfall per rainy day (RPRD; mm/day) (red) as well as the number of rainy days (NORD; days) (blue) under SSP2–4.5 and SSP5–8.5 scenarios at various global warming levels (GWLs) relative to the period 1995-2014 for each monsoon region across the 16 CMIP6 ensemble members. Shadings indicate 95% confidence intervals.*

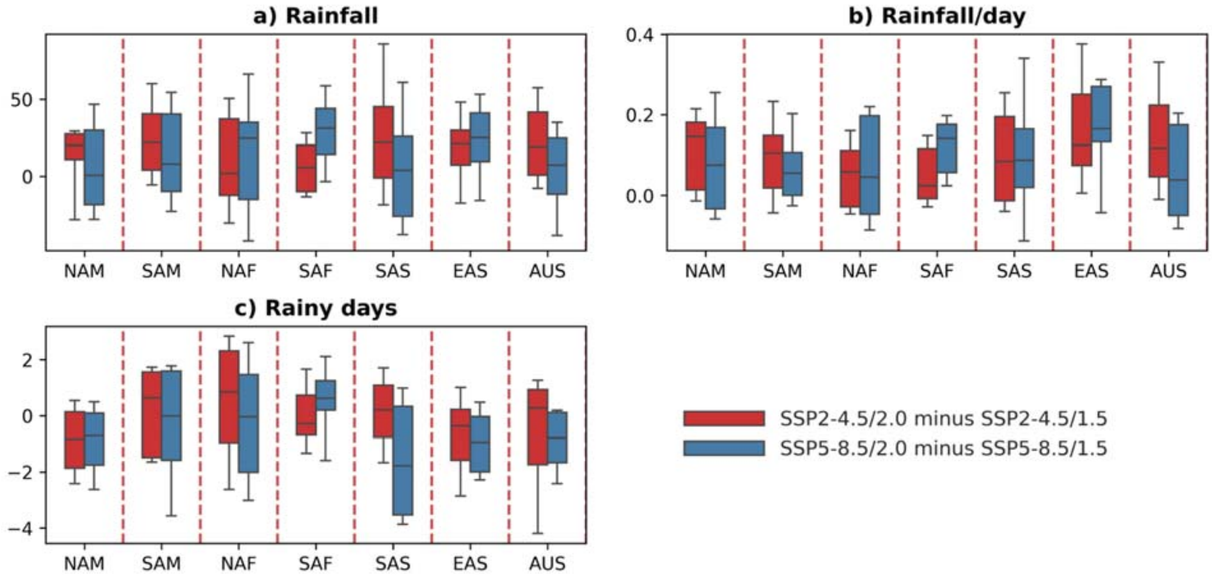


***Figure S6:*** *Changes in the area-averaged in (a) total rainfall during the rainy season (unit: mm), (b) daily rainfall rate (mm/day), and (c) number of rainy days (day) under SSP2–4.5 and SSP5–8.5 scenarios at different GWLs relative to the historical period (1995-2014) in each monsoon region. Box-and-whisker plots illustrate the 10th, 25th, 50th, 75th, and 90th percentiles.*



**Table S1:** CMIP6 model names, institution, horizontal resolution, and reference

| **Model Name** | **Institution** | **Resolution (°lon ×°lat)** | **Reference** |
|---|---|---|---|
| ACCESS-CM2 | Commonwealth Scientific and Industrial Research Organisation, Australia | 1.88 × 1.25 | Dix et al (2019a), Dix et al (2019b), Dix et al (2019c) |
| ACCESS-ESM1-5 | Commonwealth Scientific and Industrial Research Organisation, Australia | 1.88 × 1.24 | Ziehn et al (2019a), Ziehn et al (2019b), Ziehn et al (2019c) |

| | | | |
|---|---|---|---|
| CanESM5 | Canadian Earth System Model | 2.81 × 2.81 | Swart et al (2019a), Swart et al (2019b), Swart et al (2019c) |
| CESM2-WACCM | National Center for Atmospheric Research (NCAR), USA | 1.25 × 0.94 | Danabasoglu (2019a), Danabasoglu (2019b), Danabasoglu (2019c) |
| CMCC-CM2-SR5 | Euro-Mediterranean Centre on Climate Change coupled climate model, Italy | 1.25 × 0.94 | Lovato and Peano (2020a), Lovato and Peano (2020b), Lovato and Peano (2020c) |
| CMCC-ESM2 | Euro-Mediterranean Centre on Climate Change coupled climate model, Italy | 1.25 × 0.94 | Lovato and Peano (2021a), Lovato and Peano (2021b), Lovato and Peano (2021c) |
| EC-Earth3 | EC-EARTH consortium | 0.70 × 0.70 | EC-Earth (2019a), EC-Earth (2019b), EC-Earth (2019c) |
| INM-CM4-8 | Institute of Numerical Mathematics of the Russian Academy of Sciences, Russia | 2.00 × 1.50 | Volodin et al (2019a), Volodin et al (2019b), Volodin et al (2019c) |
| INM-CM5-0 | Institute of Numerical Mathematics of the Russian Academy of Sciences, Russia | 2.00 × 1.50 | Volodin et al (2019d), Volodin et al (2019e), Volodin et al (2019f) |
| IPSL-CM6A-LR | Institute Pierre-Simon Laplace (IPSL) | 2.50 × 1.26 | Boucher et al (2018), Boucher et al (2019a), Boucher et al (2019b) |
| MIROC6 | Japanese Modeling Community | 1.41 × 1.41 | Tatebe and Watanabe (2018), Shiogama et al (2019a), Shiogama et al (2019b) |
| MPI-ESM1-2-HR | Max Planck Institute | 0.94 × 0.94 | Jungclaus et al (2019), Schupfner et al (2019a), Schupfner et al (2019b) |
| MPI-ESM1-2-LR | Max Planck Institute | 1.88 × 1.88 | Wieners et al (2019a), Wieners et al (2019b), Wieners et al (2019c) |
| MRI-ESM2-0 | Meteorological Research Institute (MRI) | 1.13 × 1.13 | Yukimoto et al (2019a), Yukimoto et al (2019b), Yukimoto et al (2019c) |
| NESM3 | Nanjing University of Information Science and Technology, Nanjing, China | 1.88 × 1.88 | Cao and Wang (2019), Cao (2019a), Cao (2019c) |
| TaiESM1 | Research Center for Environmental Changes, Academia Sinica, Nankang, Taipei, Taiwan | 0.94 × 1.25 | Lee and Liang (2020a), Lee and Liang (2020b), Lee and Liang (2020c) |

## Supplementary References

Boucher, O., Denvil, S., Levavasseur, G., Cozic, A., Caubel, A., Foujols, M.-A., Meurdesoif, Y., Cadule, P., Devilliers, M., Ghattas, J., Lebas, N., Lurton, T., Mellul, L., Musat, I., Mignot, J., Cheruy, F., 2018. IPSL IPSL-CM6A-LR model output prepared for CMIP6 CMIP historical. https://doi.org/10.22033/ESGF/CMIP6.5195

Boucher, O., Denvil, S., Levavasseur, G., Cozic, A., Caubel, A., Foujols, M.-A., Meurdesoif, Y., Cadule, P., Devilliers, M., Dupont, E., Lurton, T., 2019a. IPSL IPSL-CM6A-LR model output prepared for CMIP6 ScenarioMIP ssp585. https://doi.org/10.22033/ESGF/CMIP6.5271

Boucher, O., Denvil, S., Levavasseur, G., Cozic, A., Caubel, A., Foujols, M.-A., Meurdesoif, Y., Cadule, P., Devilliers, M., Dupont, E., Lurton, T., 2019b. IPSL IPSL-CM6A-LR model output prepared for CMIP6 ScenarioMIP ssp245. https://doi.org/10.22033/ESGF/CMIP6.5264

Cao, J., 2019. NUIST NESMv3 model output prepared for CMIP6 ScenarioMIP ssp585. https://doi.org/10.22033/ESGF/CMIP6.8790

Cao, J., 2019b. NUIST NESMv3 model output prepared for CMIP6 ScenarioMIP ssp245. https://doi.org/10.22033/ESGF/CMIP6.8781

Cao, J., Wang, B., 2019. NUIST NESMv3 model output prepared for CMIP6 CMIP historical. https://doi.org/10.22033/ESGF/CMIP6.8769

Danabasoglu, G., 2019a. NCAR CESM2-WACCM model output prepared for CMIP6 CMIP historical. https://doi.org/10.22033/ESGF/CMIP6.10071

Danabasoglu, G., 2019b. NCAR CESM2-WACCM model output prepared for CMIP6 ScenarioMIP ssp585. https://doi.org/10.22033/ESGF/CMIP6.10115

Danabasoglu, G., 2019c. NCAR CESM2-WACCM model output prepared for CMIP6 ScenarioMIP ssp245. https://doi.org/10.22033/ESGF/CMIP6.10101

Dix, M., Bi, D., Dobrohotoff, P., Fiedler, R., Harman, I., Law, R., Mackallah, C., Marsland, S., O'Farrell, S., Rashid, H., Srbinovsky, J., Sullivan, A., Trenham, C., Vohralik, P., Watterson, I., Williams, G., Woodhouse, M., Bodman, R., Dias, F.B., Domingues, C.M., Hannah, N., Heerdegen, A., Savita, A., Wales, S., Allen, C., Druken, K., Evans, B., Richards, C., Ridzwan, S.M., Roberts, D., Smillie, J., Snow, K., Ward, M., Yang, R., 2019a. CSIRO-ARCCSS ACCESS-CM2 model output prepared for CMIP6 CMIP historical. https://doi.org/10.22033/ESGF/CMIP6.4271

Dix, M., Bi, D., Dobrohotoff, P., Fiedler, R., Harman, I., Law, R., Mackallah, C., Marsland, S., O'Farrell, S., Rashid, H., Srbinovsky, J., Sullivan, A., Trenham, C., Vohralik, P., Watterson, I., Williams, G., Woodhouse, M., Bodman, R., Dias, F.B., Domingues, C.M., Hannah, N., Heerdegen, A., Savita, A., Wales, S., Allen, C., Druken, K., Evans, B., Richards, C., Ridzwan, S.M., Roberts, D., Smillie, J., Snow, K., Ward, M., Yang, R., 2019b. CSIRO-ARCCSS ACCESS-CM2 model output prepared for CMIP6 ScenarioMIP ssp585. https://doi.org/10.22033/ESGF/CMIP6.4332

Dix, M., Bi, D., Dobrohotoff, P., Fiedler, R., Harman, I., Law, R., Mackallah, C., Marsland, S., O'Farrell, S., Rashid, H., Srbinovsky, J., Sullivan, A., Trenham, C., Vohralik, P., Watterson, I., Williams, G., Woodhouse, M., Bodman, R., Dias, F.B., Domingues, C.M., Hannah, N., Heerdegen, A., Savita, A., Wales, S., Allen, C., Druken, K., Evans, B., Richards, C., Ridzwan, S.M., Roberts, D., Smillie, J., Snow, K., Ward, M., Yang, R., 2019c.

CSIRO-ARCCSS ACCESS-CM2 model output prepared for CMIP6 ScenarioMIP ssp245. https://doi.org/10.22033/ESGF/CMIP6.4321

EC-Earth Consortium (EC-Earth), 2019a. EC-Earth-Consortium EC-Earth3 model output prepared for CMIP6 CMIP historical. https://doi.org/10.22033/ESGF/CMIP6.4700

EC-Earth Consortium (EC-Earth), 2019b. EC-Earth-Consortium EC-Earth3 model output prepared for CMIP6 ScenarioMIP ssp585. https://doi.org/10.22033/ESGF/CMIP6.4912

EC-Earth Consortium (EC-Earth), 2019c. EC-Earth-Consortium EC-Earth3 model output prepared for CMIP6 ScenarioMIP ssp245. https://doi.org/10.22033/ESGF/CMIP6.4880

Jungclaus, J., Bittner, M., Wieners, K.-H., Wachsmann, F., Schupfner, M., Legutke, S., Giorgetta, M., Reick, C., Gayler, V., Haak, H., de Vrese, P., Raddatz, T., Esch, M., Mauritsen, T., von Storch, J.-S., Behrens, J., Brovkin, V., Claussen, M., Crueger, T., Fast, I., Fiedler, S., Hagemann, S., Hohenegger, C., Jahns, T., Kloster, S., Kinne, S., Lasslop, G., Kornblueh, L., Marotzke, J., Matei, D., Meraner, K., Mikolajewicz, U., Modali, K., Müller, W., Nabel, J., Notz, D., Peters-von Gehlen, K., Pincus, R., Pohlmann, H., Pongratz, J., Rast, S., Schmidt, H., Schnur, R., Schulzweida, U., Six, K., Stevens, B., Voigt, A., Roeckner, E., 2019. MPI-M MPI-ESM1.2-HR model output prepared for CMIP6 CMIP historical. https://doi.org/10.22033/ESGF/CMIP6.6594

Lee, W.-L., Liang, H.-C., 2020. AS-RCEC TaiESM1.0 model output prepared for CMIP6 ScenarioMIP ssp245. https://doi.org/10.22033/ESGF/CMIP6.9808

Lee, W.-L., Liang, H.-C., 2020a. AS-RCEC TaiESM1.0 model output prepared for CMIP6 CMIP historical. https://doi.org/10.22033/ESGF/CMIP6.9755

Lee, W.-L., Liang, H.-C., 2020b. AS-RCEC TaiESM1.0 model output prepared for CMIP6 ScenarioMIP ssp585. https://doi.org/10.22033/ESGF/CMIP6.9823

Lovato, T., Peano, D., 2020a. CMCC CMCC-CM2-SR5 model output prepared for CMIP6 CMIP historical. https://doi.org/10.22033/ESGF/CMIP6.3825

Lovato, T., Peano, D., 2020b. CMCC CMCC-CM2-SR5 model output prepared for CMIP6 ScenarioMIP ssp585. https://doi.org/10.22033/ESGF/CMIP6.3896

Lovato, T., Peano, D., 2020c. CMCC CMCC-CM2-SR5 model output prepared for CMIP6 ScenarioMIP ssp245. https://doi.org/10.22033/ESGF/CMIP6.3889

Lovato, T., Peano, D., Butenschön, M., 2021a. CMCC CMCC-ESM2 model output prepared for CMIP6 CMIP historical. https://doi.org/10.22033/ESGF/CMIP6.13195

Lovato, T., Peano, D., Butenschön, M., 2021b. CMCC CMCC-ESM2 model output prepared for CMIP6 ScenarioMIP ssp585. https://doi.org/10.22033/ESGF/CMIP6.13259

Lovato, T., Peano, D., Butenschön, M., 2021c. CMCC CMCC-ESM2 model output prepared for CMIP6 ScenarioMIP ssp245. https://doi.org/10.22033/ESGF/CMIP6.13252

Schupfner, M., Wieners, K.-H., Wachsmann, F., Steger, C., Bittner, M., Jungclaus, J., Früh, B., Pankatz, K., Giorgetta, M., Reick, C., Legutke, S., Esch, M., Gayler, V., Haak, H., de Vrese, P., Raddatz, T., Mauritsen, T., von Storch, J.-S., Behrens, J., Brovkin, V., Claussen, M., Crueger, T., Fast, I., Fiedler, S., Hagemann, S., Hohenegger, C., Jahns, T., Kloster, S., Kinne, S., Lasslop, G., Kornblueh, L., Marotzke, J., Matei, D., Meraner, K., Mikolajewicz, U., Modali, K., Müller, W., Nabel, J., Notz, D., Peters-von Gehlen, K., Pincus, R., Pohlmann, H., Pongratz, J., Rast, S., Schmidt, H., Schnur, R., Schulzweida, U., Six, K., Stevens, B., Voigt, A., Roeckner, E., 2019a. DKRZ MPI-ESM1.2-HR model output prepared for CMIP6 ScenarioMIP ssp585. https://doi.org/10.22033/ESGF/CMIP6.4403

Schupfner, M., Wieners, K.-H., Wachsmann, F., Steger, C., Bittner, M., Jungclaus, J., Früh, B., Pankatz, K., Giorgetta, M., Reick, C., Legutke, S., Esch, M., Gayler, V., Haak, H., de Vrese, P., Raddatz, T., Mauritsen, T., von Storch, J.-S., Behrens, J., Brovkin, V., Claussen, M., Crueger, T., Fast, I., Fiedler, S., Hagemann, S., Hohenegger, C., Jahns, T., Kloster, S., Kinne, S., Lasslop, G., Kornblueh, L., Marotzke, J., Matei, D., Meraner, K., Mikolajewicz, U., Modali, K., Müller, W., Nabel, J., Notz, D., Peters-von Gehlen, K., Pincus, R., Pohlmann, H., Pongratz, J., Rast, S., Schmidt, H., Schnur, R., Schulzweida, U., Six, K., Stevens, B., Voigt, A., Roeckner, E., 2019b. DKRZ MPI-ESM1.2-HR model output prepared for CMIP6 ScenarioMIP ssp245. https://doi.org/10.22033/ESGF/CMIP6.4398

Shiogama, H., Abe, M., Tatebe, H., 2019a. MIROC MIROC6 model output prepared for CMIP6 ScenarioMIP ssp585. https://doi.org/10.22033/ESGF/CMIP6.5771

Shiogama, H., Abe, M., Tatebe, H., 2019b. MIROC MIROC6 model output prepared for CMIP6 ScenarioMIP ssp245. https://doi.org/10.22033/ESGF/CMIP6.5746

Swart, N.C., Cole, J.N.S., Kharin, V.V., Lazare, M., Scinocca, J.F., Gillett, N.P., Anstey, J., Arora, V., Christian, J.R., Jiao, Y., Lee, W.G., Majaess, F., Saenko, O.A., Seiler, C., Seinen, C., Shao, A., Solheim, L., von Salzen, K., Yang, D., Winter, B., Sigmond, M., 2019a. CCCma CanESM5 model output prepared for CMIP6 CMIP historical. https://doi.org/10.22033/ESGF/CMIP6.3610

Swart, N.C., Cole, J.N.S., Kharin, V.V., Lazare, M., Scinocca, J.F., Gillett, N.P., Anstey, J., Arora, V., Christian, J.R., Jiao, Y., Lee, W.G., Majaess, F., Saenko, O.A., Seiler, C., Seinen, C., Shao, A., Solheim, L., von Salzen, K., Yang, D., Winter, B., Sigmond, M., 2019b. CCCma CanESM5 model output prepared for CMIP6 ScenarioMIP ssp585. https://doi.org/10.22033/ESGF/CMIP6.3696

Swart, N.C., Cole, J.N.S., Kharin, V.V., Lazare, M., Scinocca, J.F., Gillett, N.P., Anstey, J., Arora, V., Christian, J.R., Jiao, Y., Lee, W.G., Majaess, F., Saenko, O.A., Seiler, C., Seinen, C., Shao, A., Solheim, L., von Salzen, K., Yang, D., Winter, B., Sigmond, M., 2019c. CCCma CanESM5 model output prepared for CMIP6 ScenarioMIP ssp245. https://doi.org/10.22033/ESGF/CMIP6.3685

Tatebe, H., Watanabe, M., 2018. MIROC MIROC6 model output prepared for CMIP6 CMIP historical. https://doi.org/10.22033/ESGF/CMIP6.5603

Volodin, E., Mortikov, E., Gritsun, A., Lykossov, V., Galin, V., Diansky, N., Gusev, A., Kostrykin, S., Iakovlev, N., Shestakova, A., Emelina, S., 2019a. INM INM-CM4-8 model output prepared for CMIP6 CMIP historical. https://doi.org/10.22033/ESGF/CMIP6.5069

Volodin, E., Mortikov, E., Gritsun, A., Lykossov, V., Galin, V., Diansky, N., Gusev, A., Kostrykin, S., Iakovlev, N., Shestakova, A., Emelina, S., 2019b. INM INM-CM4-8 model output prepared for CMIP6 ScenarioMIP ssp585. https://doi.org/10.22033/ESGF/CMIP6.12337

Volodin, E., Mortikov, E., Gritsun, A., Lykossov, V., Galin, V., Diansky, N., Gusev, A., Kostrykin, S., Iakovlev, N., Shestakova, A., Emelina, S., 2019d. INM INM-CM5-0 model output prepared for CMIP6 CMIP historical. https://doi.org/10.22033/ESGF/CMIP6.5070

Volodin, E., Mortikov, E., Gritsun, A., Lykossov, V., Galin, V., Diansky, N., Gusev, A., Kostrykin, S., Iakovlev, N., Shestakova, A., Emelina, S., 2019e. INM INM-CM5-0 model output prepared for CMIP6 ScenarioMIP ssp585. https://doi.org/10.22033/ESGF/CMIP6.12338

Volodin, E., Mortikov, E., Gritsun, A., Lykossov, V., Galin, V., Diansky, N., Gusev, A., Kostrykin, S., Iakovlev, N., Shestakova, A., Emelina, S., 2019c. INM INM-CM4-8 model output prepared for CMIP6 ScenarioMIP ssp245. https://doi.org/10.22033/ESGF/CMIP6.12327

Volodin, E., Mortikov, E., Gritsun, A., Lykossov, V., Galin, V., Diansky, N., Gusev, A., Kostrykin, S., Iakovlev, N., Shestakova, A., Emelina, S., 2019f. INM INM-CM5-0 model output prepared for CMIP6 ScenarioMIP ssp245. https://doi.org/10.22033/ESGF/CMIP6.12328

Wieners, K.-H., Giorgetta, M., Jungclaus, J., Reick, C., Esch, M., Bittner, M., Legutke, S., Schupfner, M., Wachsmann, F., Gayler, V., Haak, H., de Vrese, P., Raddatz, T., Mauritsen, T., von Storch, J.-S., Behrens, J., Brovkin, V., Claussen, M., Crueger, T., Fast, I., Fiedler, S., Hagemann, S., Hohenegger, C., Jahns, T., Kloster, S., Kinne, S., Lasslop, G., Kornblueh, L., Marotzke, J., Matei, D., Meraner, K., Mikolajewicz, U., Modali, K., Müller, W., Nabel, J., Notz, D., Peters-von Gehlen, K., Pincus, R., Pohlmann, H., Pongratz, J., Rast, S., Schmidt, H., Schnur, R., Schulzweida, U., Six, K., Stevens, B., Voigt, A., Roeckner, E., 2019a. MPI-M MPI-ESM1.2-LR model output prepared for CMIP6 CMIP historical. https://doi.org/10.22033/ESGF/CMIP6.6595

Wieners, K.-H., Giorgetta, M., Jungclaus, J., Reick, C., Esch, M., Bittner, M., Gayler, V., Haak, H., de Vrese, P., Raddatz, T., Mauritsen, T., von Storch, J.-S., Behrens, J., Brovkin, V., Claussen, M., Crueger, T., Fast, I., Fiedler, S., Hagemann, S., Hohenegger, C., Jahns, T., Kloster, S., Kinne, S., Lasslop, G., Kornblueh, L., Marotzke, J., Matei, D., Meraner, K., Mikolajewicz, U., Modali, K., Müller, W., Nabel, J., Notz, D., Peters-von Gehlen, K., Pincus, R., Pohlmann, H., Pongratz, J., Rast, S., Schmidt, H., Schnur, R., Schulzweida, U., Six, K., Stevens, B., Voigt, A., Roeckner, E., 2019b. MPI-M MPI-ESM1.2-LR model output prepared for CMIP6 ScenarioMIP ssp585. https://doi.org/10.22033/ESGF/CMIP6.6705

Wieners, K.-H., Giorgetta, M., Jungclaus, J., Reick, C., Esch, M., Bittner, M., Gayler, V., Haak, H., de Vrese, P., Raddatz, T., Mauritsen, T., von Storch, J.-S., Behrens, J., Brovkin, V., Claussen, M., Crueger, T., Fast, I., Fiedler, S., Hagemann, S., Hohenegger, C., Jahns, T., Kloster, S., Kinne, S., Lasslop, G., Kornblueh, L., Marotzke, J., Matei, D., Meraner, K., Mikolajewicz, U., Modali, K., Müller, W., Nabel, J., Notz, D., Peters-von Gehlen, K., Pincus, R., Pohlmann, H., Pongratz, J., Rast, S., Schmidt, H., Schnur, R., Schulzweida, U., Six, K., Stevens, B., Voigt, A., Roeckner, E., 2019c. MPI-M MPI-ESM1.2-LR model output prepared for CMIP6 ScenarioMIP ssp245. https://doi.org/10.22033/ESGF/CMIP6.6693

Yukimoto, S., Koshiro, T., Kawai, H., Oshima, N., Yoshida, K., Urakawa, S., Tsujino, H., Deushi, M., Tanaka, T., Hosaka, M., Yoshimura, H., Shindo, E., Mizuta, R., Ishii, M., Obata, A., Adachi, Y., 2019a. MRI MRI-ESM2.0 model output prepared for CMIP6 CMIP historical. https://doi.org/10.22033/ESGF/CMIP6.6842

Yukimoto, S., Koshiro, T., Kawai, H., Oshima, N., Yoshida, K., Urakawa, S., Tsujino, H., Deushi, M., Tanaka, T., Hosaka, M., Yoshimura, H., Shindo, E., Mizuta, R., Ishii, M., Obata, A., Adachi, Y., 2019b. MRI MRI-ESM2.0 model output prepared for CMIP6 ScenarioMIP ssp585. https://doi.org/10.22033/ESGF/CMIP6.6929

Yukimoto, S., Koshiro, T., Kawai, H., Oshima, N., Yoshida, K., Urakawa, S., Tsujino, H., Deushi, M., Tanaka, T., Hosaka, M., Yoshimura, H., Shindo, E., Mizuta, R., Ishii, M., Obata, A., Adachi, Y., 2019c. MRI MRI-ESM2.0 model output prepared for CMIP6 ScenarioMIP ssp245. https://doi.org/10.22033/ESGF/CMIP6.6910

Ziehn, T., Chamberlain, M., Lenton, A., Law, R., Bodman, R., Dix, M., Wang, Y., Dobrohotoff, P., Srbinovsky, J., Stevens, L., Vohralik, P., Mackallah, C., Sullivan, A., O'Farrell, S., Druken, K., 2019a. CSIRO ACCESS-ESM1.5 model output prepared for CMIP6 CMIP historical. https://doi.org/10.22033/ESGF/CMIP6.4272

Ziehn, T., Chamberlain, M., Lenton, A., Law, R., Bodman, R., Dix, M., Wang, Y., Dobrohotoff, P., Srbinovsky, J., Stevens, L., Vohralik, P., Mackallah, C., Sullivan, A., O'Farrell, S., Druken, K., 2019b. CSIRO ACCESS-ESM1.5 model output prepared for CMIP6 ScenarioMIP ssp585. https://doi.org/10.22033/ESGF/CMIP6.4333

Ziehn, T., Chamberlain, M., Lenton, A., Law, R., Bodman, R., Dix, M., Wang, Y., Dobrohotoff, P., Srbinovsky, J., Stevens, L., Vohralik, P., Mackallah, C., Sullivan, A., O'Farrell, S., Druken, K., 2019c. CSIRO ACCESS-ESM1.5 model output prepared for CMIP6 ScenarioMIP ssp245. https://doi.org/10.22033/ESGF/CMIP6.4322